Universidad de Zaragoza

Master thesis

Máster Universitario en Materiales Nanoestructurados para Aplicaciones Nanotecnológicas (NANOMAT)

Creating covalent nanostructures for magnetoelectronic applications.

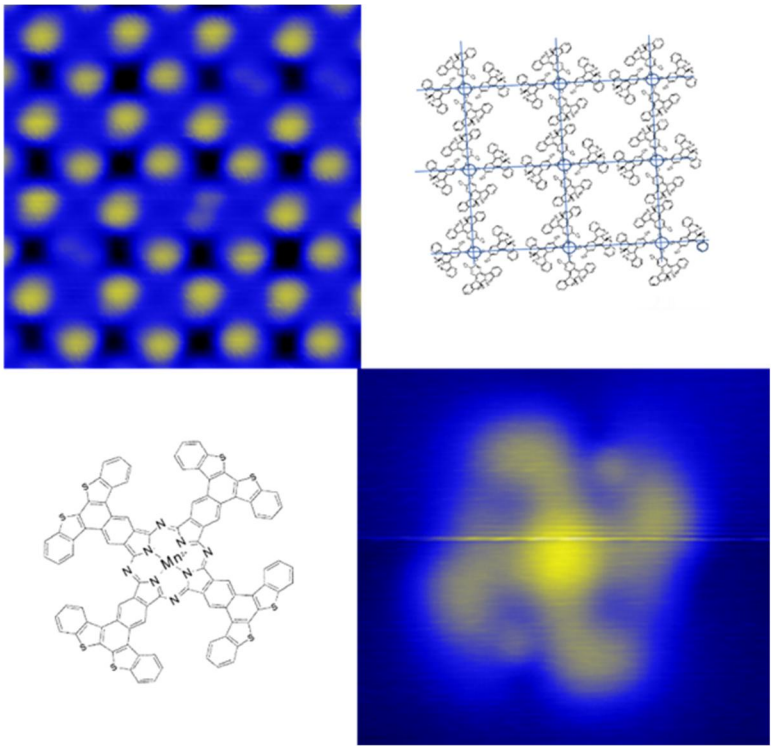

Carlos Casas Carretero

Supervised by: Dr. David Serrate Donoso and Dr. Joge Lobo Checa.

Instituto de Nanociencia de Aragón

December 2017

INDICE:

1- MOTIVATION:

1.1 On surface synthesis.

On surface synthesis is the bottom-up fabrication of 2D nanostructures stemming from covalent molecular assemblies on solid surfaces, performing the reactions directly on the surface. Therefore, molecular structures are governed by molecule-surface interactions and direct molecule-molecule bonds. [1]

On-surface synthesis constitutes a rapidly growing field of research due to its promising application for creating stable molecular structures on surfaces. [2] While self-assembled structures rely on reversible interactions, on-surface synthesis provides the potential for creating long-term stable structures with well-controlled properties. [3] Performing the reactions directly on the surface provides a great potential for surface functionalization and the creation of functional devices.

On-surface synthesis offers the possibility to prepare compounds that cannot be synthesized in solution due to solubility issues. On-surface reactions can be realized without introducing solvents and under ultra-high vacuum conditions, which permits utmost control over the purity of products. The absence of solvents also offers a much larger range of reaction temperatures. The two-dimensional confinement of the molecules on the surface can be deliberately employed for stabilizing transient structures, which offers the potential to explore entirely new reaction pathways. [4] To exploit the benefits of on-surfaces synthesis a detailed insight into the molecule–surface interaction and the specific adsorption geometry is required. Extended structures (symmetry, hierarchy, and coordination numbers) can be designed by balancing between a lateral metal–ligand interaction and a vertical molecule–substrate interaction. [5] For the investigation of these reactions, scanning probe techniques constitute a most valuable tool, since they allow us to directly image the precursors and their resulting products with sub-molecular resolution in real space. [5]

Metal surfaces exhibit several advantages for on-surface synthesis. First, organic precursor molecules typically anchor firmly to metal surface, permitting the use of annealing treatments to trigger the reactions. Second, metal surfaces have been shown to promote the on-surface reaction by acting as a catalyst. The reactivity of the surface is highly dependent on the crystal facet used (surface termination planes) and on the type of metal. The surface electronic structure plays an

important role because it lowers the diffusion energy barrier, improving the ability of different precursors to find each other across the surface. An important parameter that determines the kind of structures that will be formed upon deposition depends on whether the process is driven by kinetics or thermodynamics. [6]

1.2 An on-surface synthesis case: Phthalocyanines generated by cyclotetramerization of precursors.

Often, it is not feasible to incorporate in a single molecule all the necessary end-groups for a reaction either because they cannot be synthesized in solution or because they are too large to be evaporated without breaking into fragments before being adsorbed on the surface. In these cases, co-deposition of two species can help to overcome these limitations and can even trigger the reaction without the need of annealing. Although this process is more challenging from the preparation side, new products and structures can be obtained that are otherwise unachievable. An example of this is the generation of Phthalocyanines by cyclotetramerization of smaller precursors.

Phthalocyanines are two-dimensional 18 π-electron aromatic porphyrin (Por) synthetic analogues, consisting of four isoindole subunits linked together through nitrogen atoms**.** [7] Numerous properties arise from their electronic delocalization, which makes them valuable in different fields of science and technology. The chemical flexibility of this class of compounds allows the preparation of a large variety of related structures and, consequently, the tailoring of the physical, electronic, and optical properties, as well as the improvement of the processability. [8]

Phthalocyanines are usually prepared by cyclotetramerization of phthalonitriles or their derivatives [9]. The on-surface confined synthesis allows the preparation of molecular architectures of this kind that cannot be synthesized in solution. [10] Piantek *et al.* showed that this cyclotetramerization is possible on surfaces. [11] A part of this Master thesis deals precisely with the formation of a Mn-Phthalocyanine derivative that contains optically switchable units in its structure, which will be described in detail in section 3.1.

1.3 Influence of metallic substrate upon molecular orbitals.

On-surface synthesis generally takes places on metallic surfaces, thus it is important to understand the interactions with the molecular precursors. In this way, we must revisit the existing electronic differences between an inorganic and an organic material. While inorganic (metallic) materials feature valence bands formed by a continuum of states characterized by delocalized

electrons, (non-polymeric) organics materials are composed by discrete, non-dispersive levels when isolated or in the gas phase. Every level is associated to a molecular orbital that can be either strongly localized on an end-group or a constitutional unit of the molecule, or delocalized over a large part of it. The two main orbitals that are involved in the charge transport are the "Highest Occupied Molecular Orbital" (HOMO) and the "Lowest Unoccupied Molecular Orbital" (LUMO) that are separated by a defined energy gap, analogous to the valence and conduction bands of insulators or semiconductors.

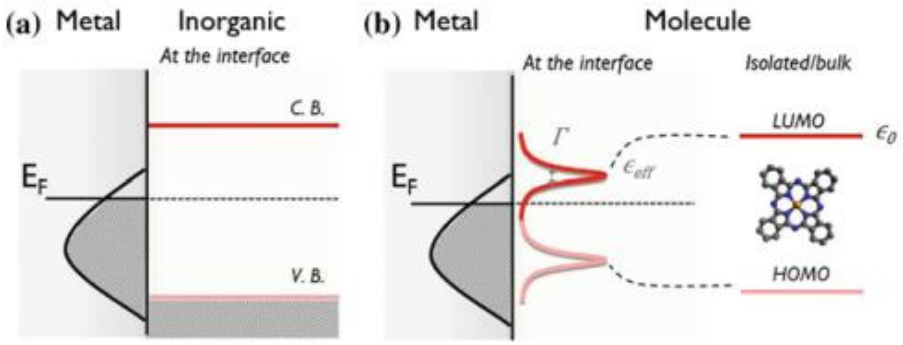

Fig 1.1. Schematic representation of a) the interface between a metal and an inorganic material such as a semiconductor or insulator versus b) the event when an isolated molecule is brought in proximity with a metallic surface. For simplicity, a flat band configuration is used for the semiconductor in the first few nanometers from the interface. Adapted from Ref. [12].

When a molecule is brought in proximity to a metallic electrode, the initially isolated molecular levels are progressively hybridized by coupling with the available metallic states (Fig. 1.1). This leads to two main effects:

1- The lifetime (τ) of the molecular level becomes finite since the charge has a certain probability to decay into the metal. Consequently, the energy δE is no longer completely defined, resulting in energy level broadening with a finite width $\Gamma \approx \hbar/\tau$, which in first approximation, is proportional to the density of states (DOS) of the metal.

2- In addition, an energy shift of the molecular level from the initial position of the isolated molecule ε_0 to the final one ε_{ff} occurs by the interaction with the metal. This energy renormalization is dependent on the metal DOS and includes, among other contributions, the combined effects of interfacial dipoles or image forces. [12]

2 - EXPERIMENTAL TECHNIQUES.

2.1 Sample preparation: Co-evaporation in Ultra High Vacuum.

On-surface synthesis requires atomically clean substrates to serve as basis for the molecular reactions. Therefore, the use of ultra-high vacuum (UHV) environments is essential to attain atomically precise control on the resulting structures [13]. Indeed, most surface science experiments are performed under UHV for two reasons:

1- To achieve mean free paths of probe and detected particles (ions, atoms, electrons) significantly greater than the dimensions of the apparatus. This is a requisite for surface spectroscopies, which must avoid collisions with residual gas phase molecules.

2- To gain reproducibility, avoid sample contamination, and ensure sample cleanliness during the duration of the experiment. The contribution of background gas adsorption is therefore reduced to a minimum, even for reactive surfaces.

In UHV we obtain atomically clean metallic surfaces by repeated cycles of Ar^+ ion sputtering and annealing. This treatment has been applied to a silver (111) monocrystal, where cleanliness of the fresh surface was confirmed from the observation of its characteristic surface state.

The molecular deposition is generally done by thermal sublimation from a Knudsen cell that is heated by a resistive filament. Such cells utilize the principle of molecular effusion, where the solid material to be deposited is heated until it reaches a suitable vapor pressure in an isothermal enclosure. The deposition rate is extremely stable and determined by the crucible temperature. [14] To monitor the deposition rate along the process, we used a quartz crystal microbalance controller.

Our molecular evaporator consisted of a filament wound up around the molecular crucible. The current used was such that it allowed our cell to reach its evaporation temperatures (in this case close to ~105ºC), yielding constant deposition rates of 0.04 ML/min monitored by a quartz microbalance attached at the end of the cell (1 ML (monolayer) corresponds to covering the whole surface by a complete layer of the self-assembled molecules).

The metal evaporation is done by electron bombardment of the material, usually known as e-beam heating. This method is used when higher temperatures need to be reached. In this process, the electrons generated from a hot filament are accelerated by a positive electric field (of the order

of 1 kV) which focus them into the crucible that contains the material to be evaporated. The kinetic energy of the electron beam is transferred to the material container, which causes the increase of temperature until evaporation conditions are reached. [14] Specifically, we used 6.8 mA of emission current and 650 V of high voltage to obtain a rate of 0.002 ML/min. (1 ML corresponds to the deposition of one atom of Mn in every unit cell of the Ag surface).

When two species are deposited upon a clean substrate, it is generally done by sequential evaporation. It consists in a step-by-step deposition of the components generally followed by annealing to activate the on-surface reaction. This self-assembly process depends upon the kinetics and stability of the elements of the system. Generally, sequential deposition leads to stoichiometric mixing of the elements. However, sometimes it leads to the generation of stable mono-species domains that prevents the components from mixing, hindering the on-surface reactions. To avoid such limitation simultaneous evaporation of the two species (co-evaporation) must be done, which consists in a controlled deposition of both components.

For our experiments, we co-evaporated Mn and Dicyanodiarylethene (DCDAE) monomers (Fig 2.1) as precursors on a Ag (111) surface. The molecules were provided by the group of Diego Peña at University of Santiago de Compostela. A coordinated phase results from the co-deposition at room temperature (RT). However, when the sample is annealed at 360ºC cyclotetramerization of the momomer around a Mn ion occurs, which produces a phthalocyanine derivative with rotational units. Both of these structures as well as their local electronic signatures will be discussed in depth in the results section.

DCDAE is a monomer that consists of a diarylethene scaffold to which two cyano groups are added at one end that are responsible for the generation of covalent bonds with the manganese ion after the cyclotetramerization process. An important characteristic of this molecule is the presence of hydrogen atoms linked to the aromatic rings at the other end of the cyano groups since it hinders the planar absorption geometry of the background carbon.

Diarylethene are well-known photochromic compounds since reactions take place between two isomers (hexatriene and cyclohexadiene) where color changes are attributed to the different electrical structures between the open-ring and closed-ring structures (see Fig. 2.1).[16]

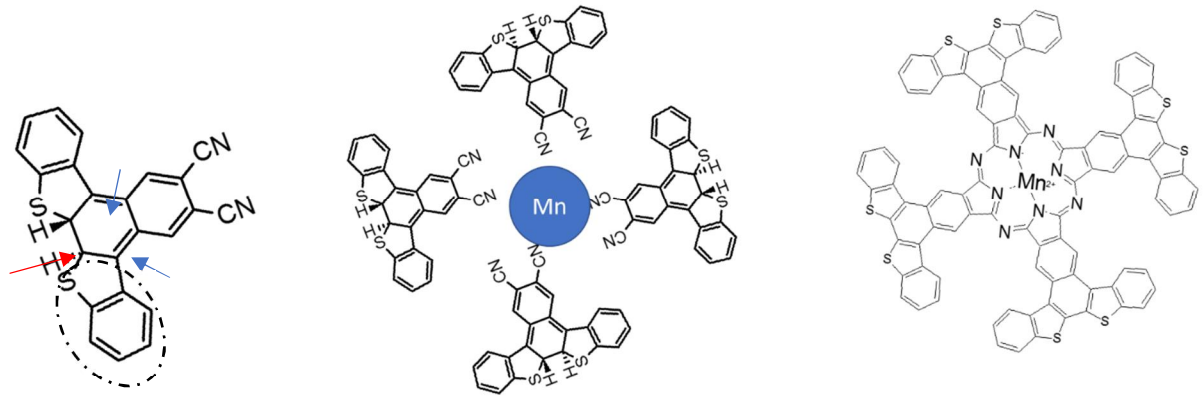

Fig 2.1. Schematic representation of Dicyanodiarylethene (DCDAE) *molecule (left) and the compounds formed in this work: coordinated phase with Mn atoms (center) and phthalocyanine dericative after cyclotetramerization (right) by annealing the middle phase to 360ºC. The C-C bond indicated by the red arrow can open and close defining two possible isomers. In its open form, the bonds indicated by the blue arrows become single sigma-bonds, and the thiophene ring (the one containing sulphur) can rotate freely around this axis with the only constrain of the interaction with the surface.*

To summarize, the aim of this master project is to **covalently link metal ions to generate optically active ligands**, creating a hybrid with new magnetic, optical and transport properties. In particular, the right of figure 2.1 shows the new molecule fabricated with the following characteristics: 1) it cannot be synthesized in solution; 2) magnetic and transport properties will have strong dependence on optical stimuli exerted; 3) inversely, the optoelectronic response of this molecule will depend on the magnetic state of the ion; 4) the method is likely more general as we could 4.1) exchange the metal ion or 4.2) add further reactivity to the monomer to have 2D extended covalent metalorganic lattice with optoelectronic functionality.

2.2 Scanning Tunneling Microscopy (STM).

The technique of choice to study the prepared samples is Scanning Tunneling Microscopy (STM). [17] It was used in both topographic in spectroscopic modes (the latter will be described in the next subsection). The STM consists of a sharp metallic tip that approaches vertically a flat, conducting sample and is laterally scanned along the surface by piezoelectric actuators. Once both electrodes (sample and tip) are in contact a current can flow upon applying a voltage.

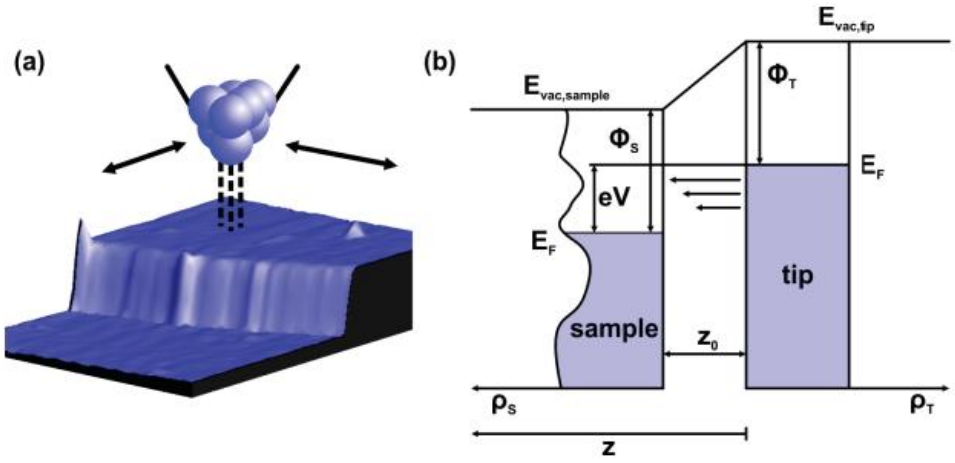

Fig 2.2. (a) Schematic view of a sample–tip tunnel junction. The tip is laterally scanned over the surface. The tunneling electrons flow between the terminating tip atom and the surface (indicated with dashed lines). b) Sketch of the tunneling process. A bias voltage V is applied to the sample, which shifts the Fermi energy (E_F) by eV relative to the tip. The electrons can tunnel through the vacuum (width z_0) from occupied states from the tip (constant density of states ρ_T) into empty states in the sample (density of states denoted by ρ_S). Note that electrons close to the Fermi energy of the tip contribute most to the tunneling current (indicated by the lengths of black arrows) due to the tunneling matrix element M. Figure adapted from Ref [18].

However, already at a very small distance between sample and tip (some Å apart from each other), a tiny current (in the range of nanoamperes) can also flow (indicated by the dashed lines in Figure 2.2.a). This so-called tunneling current is based on quantum tunneling effects and can be described by quantum mechanics (detailed theory can be found in Appendix 1).

The tunneling current depends exponentially on the small distance between sample and tip, which is a prerequisite for the high spatial resolution of STM. Due to this dependence, only the terminating atoms of the tip are significantly contributing to the tunneling current. [18]

There are two main operation modes for topographic acquisition in STM. First, in constant-current mode the tip is laterally scanned over the surface while the tunneling current is held constant at a certain set-point current I_0. Depending on the lateral position of the tip the tunneling current can deviate from I_0. The current is kept constant at I_0 by adjusting the tip sample distance as the control parameter of a feedback loop. In this way, recording the feedback response for each lateral position of the scanner, a topographic rendering of the sample can be retrieved. In the second

mode, constant-height, the tip is simply scanned laterally over the surface while the tunneling current is recorded as a function of its lateral position $I(x, y)$. This is usually accomplished by switching off the feedback loop. In this mode image can be acquired much faster, but there is a high risk of crashing the tip on the surface due to any existing corrugation. In exchange, the image obtained is a spatially resolved map of the density of states, rather than a structural topography. For our experiments, we used the constant-current mode for the topographic images and constant height mode for dV/dI maps at different bias voltage.

2.3 Scanning Tunneling Spectroscopy (STS). Cryogenic conditions.

Scanning tunneling spectroscopy (STS) is an acquisition mode of STM that consists in recording the differential conductance as a function of the bias voltage. While in topography the tip is scanned in the x-y-plane over the surface of the sample, in STS the tip (at constant height) is placed on top of a feature of interest (adatom, molecule or step edge) and the (bias) voltage is swept over an energy range while the feedback loop is turned off (open feedback) (figure 2.3). In this way, I/V curves are measured and its first derivative, that is the differential conductance (dI/dV), is proportional to the local density of states (LDOS) of the sample (n_s). [19] The differential conductance can be written as:

$$\left.\frac{\partial I_T}{\partial V}\right|_V \propto n_t \int_{-\infty}^{\infty} n_s(\vec{r_0}, \epsilon)\delta(\epsilon - eV)d\epsilon = n_t n_s(\vec{r_0}, eV).$$

From this equation, it can be extracted that the $\partial I_T / \partial V$ gives a value proportional to the sample LDOS at the tip position r_0 and energy eV, where e is elementary charge unit and V the applied bias voltage.

The acquisition of accurate dI/dV curves demands better thermal and mechanical stability than topographic images to reduce the noise of its derivative. To this end, STS is done at strict cryogenic conditions (usually liquid He (4K) or lower), which bear the benefit of strongly limiting surface diffusion of physisorbed species, and attenuating significantly any thermal drift. Indeed, cryogenic temperatures are also essential for STM manipulation of individual atoms and molecules and enables the use of the STM tip to access and manipulate individual chemical bonds in a controlled way. Furthermore, by reducing thermal broadening of the probing electronic energy

distribution, spectroscopic resolution is improved. Through STS and inelastic electron tunneling spectroscopy, the cryogenic UHV STM is recurrently used as a tool for the chemical identification of individual adsorbed molecular species and for obtaining the intra-molecular and intra-atomic electronic structure of both randomly adsorbed molecules and patterned arrays [20].

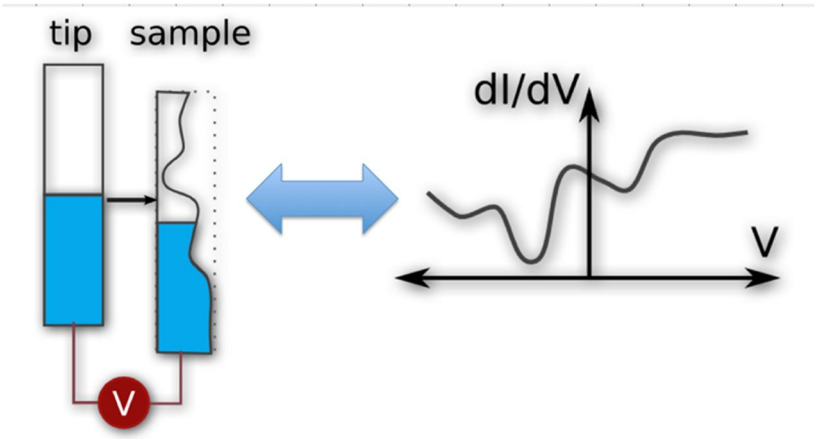

Fig 2.3. Scanning Tunneling Spectroscopy schematic representation. A bias voltage (V) is applied between sample and tip that generates a current (I). Its derivative (dI/dV) is represented versus V obtaining the LDOS of the object.
Figure adapted from http://lair.phas.ubc.ca/techniques/scanning-tunnelling-microscopy/

3- RESULTS

In this chapter, through STM and STS measurements we explore in detail the morphology and electronic configuration in both the coordinated phase and the MnDCDAE molecules resulting after the cyclotetramerization process. Moreover, we use the STM tip as a tool to perform manipulation upon these systems. In consequence, this section will be divided into two parts: the first dealing with assemblies before the on-surface synthesis (the coordinated phase), and the second, centered in the products after the reaction (the MnDCDAE monomers). Note that the absence of Mn atoms on the Ag(111) surface leads to a completely different and purely organic phase bonded by weak Van der Waals interactions, what is commonly known as a self-assembled monolayer (see Appendix 3).

3.1- COORDINATED PHASE.

3.1.1 Topography.

In situ co-evaporation of DCDAE monomers and Mn on a Ag(111) single crystal surface results in a two-dimensional metal−organic network. The Mn atoms and DCDAE molecules form regular squared structures (see Fig. 3.1). Although at low coverages the Ag step edges are decorated, the majority of the ordered structures occur directly on the terraces, forming large, rectangular islands. The square packing geometry presents two equal unit lattice vectors of 2.00 ± 0.05 nm. Up to three different orientational domains can be observed on a single terrace. This is induced by the different symmetry between network and substrate, since the surface is three-fold (120º rotational symmetry) whereas the molecular assembly has four-fold symmetry (90º rotational symmetry). This reveals that the interaction with the substrate plays a primary role in the stabilization of a single phase with unique crystallographic registry with the surface lattice.

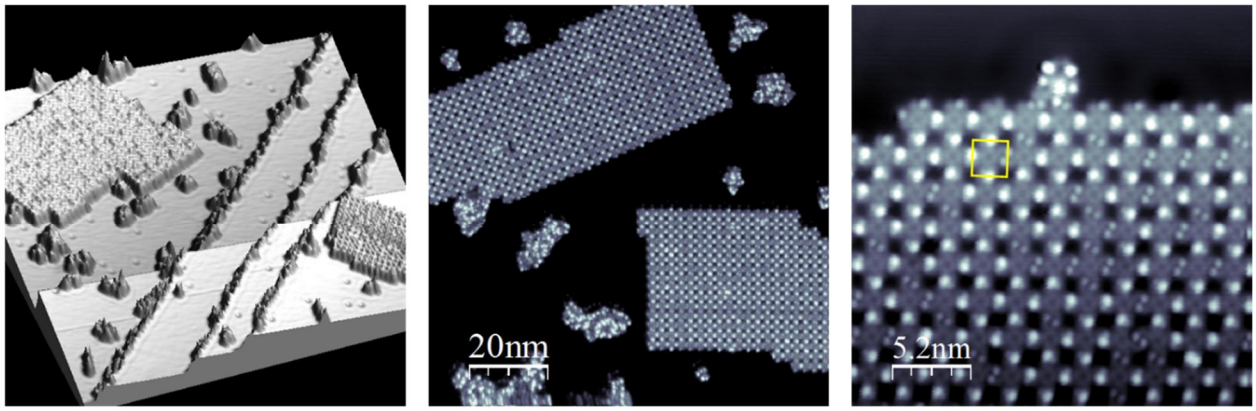

Figure 3.1. Topography of the Mn + DCDAE coordinated phase. a) 3D topographic image showing step decoration and well defined rectangular islands at the center of the terraces. b) STM image showing two square structures with different orientations in the same terrace. c) High resolution image of a single square structure domain. The square unit cell is included in the image with the Mn atoms at their center (marked by a intensity depression). STM parameters: a) V =100mV , I = 50 pA; b) V=600mV, I= 90pA; c) V=100mV, I=50 pA

This four-fold assembly is stabilized through a combination of cyano groups with single Mn atoms and hydrogen bonds to neighboring molecules, as showed in Fig. 3.2. In this structure, each Mn atom can be visualized as a round darker feature that connects to four organic ligands in an orthogonal fashion. Therefore, each single Mn ion is surrounded by four CN groups (each

belonging to a different DCDAE molecule) forming tetramer structures. Every tetramer within the square network is weekly bonded to four other neighboring tetramers forming a so-called surface-confined metal–organic networks (SMONs) (fig 3.1 and 3.2). Full description of the bonding process can be found in Appendix 2.

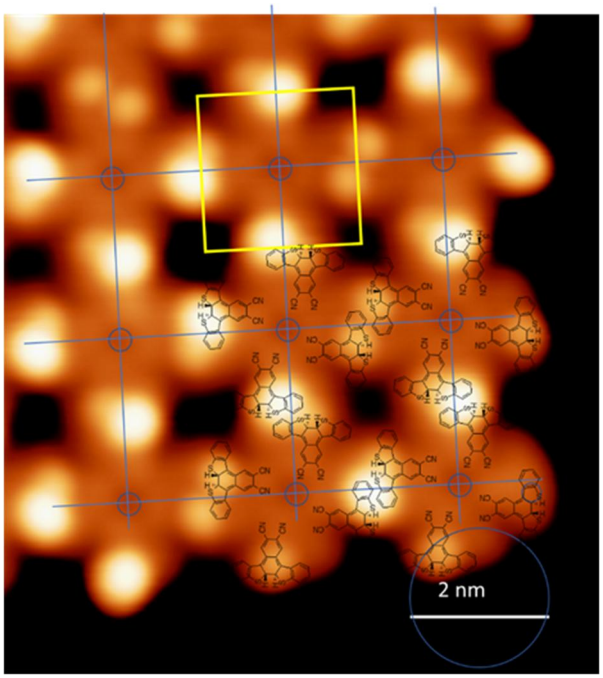

Fig 3.2 Topography of coordinated network detail. Square unit cell (in yellow) with Mn atoms indicated by circles. Coordinative bonds require that the cyano groups are in contact with the metal ions, and consequently the round lobes with bimodal size distribution must be located near to the sulphur atoms and the optically active C-C bond (see Fig. 2.1). STM regulation: V=-500 mV, I = 42 pA.

It is important to note that between every neighboring Mn atoms, at the edges of the unit cells, bright features are always observed. This coincides spatially with the diarylethene part of the molecule opposite to the cyano groups (see Fig 2.1). A visual inspection shows that these bright features appear in pairs, suggesting that each of them belongs to one of the thiophene rings, and that there are two types of these. The strong contrast between big and small lobes at the sulphur sites can be interpreted in two ways: (i) as due to changes in the position of the non-planar H atoms in the vicinity of the sulphur atoms; or (ii) as a fingerprint of the existence of the two isomers (open and closed, see Fig. 2.1), suggesting that the optical functionality remains at the coordinated phase.

Both interpretations influence the planarity of the molecules with respect to the surface. In a topography image as in Fig. 3.2 it is tempting to assign the brighter and bigger lobes to structures which are just above the molecular plane, and those appearing smaller to structures at the molecule plane, and therefore closer to the surface. Note that due to steric reasons, the hydrogen atoms

depicted in Fig. 3.2 belonging to the same molecule cannot be at the same height, irrespective of its isomer configuration with open or closed ring status.

However, as depicted in Fig. 2.2, any STM topography carries the information of the electronic structure averaged between the Fermi level and the tunneling bias. This compromises the identification of individual molecular orbitals lying at certain energies (see Fig. 1.1), which is the key tool to assign a given molecular structure to the coordinated phase. In the following, we will analyze the electronic structure and bond character of the metal−organic networks, after conducting STS measurements at liquid-He temperature.

3.1.2. Electronic structure. Spectroscopy, maps, open and close molecules.

In this square network, the presence of Mn ions is the driving force for the coordinated phase structure, since metallic bonds form when the electronic states of the molecular end-groups (cyanos in our case) interact with the valence states of the Mn. Experimentally, this is confirmed by the inexistence of the squared mesh when DCDAE precursors are deposited without Mn atoms (appendix 3). The valence band of Mn is composed of a broad s-electron band plus a sharp d-electron band. The broad metallic s-band is similar to most of the transition metals featuring a single electron. Therefore, the coupling of the adsorbate states with the half-filled s-band result is a broadening and a shift of the molecular states. However, the narrow d-band changes its occupancy for the different transition metals, which finally determines the chemical bond, and consequently its catalytic activity. In particular, the strong coupling of the adsorbate states with the sharp d-band leads to a splitting of those states, developing bonding and anti-bonding molecular electronic states.

Several parameters define the activity of the d-band: i) the density of states at the Fermi level (E_F) that determines the ability of a surface to react with different molecules (electrons at E_F are energetically prone for bonding); ii) the number of d-holes related to the empty d-states above E_F because the unoccupied states play an important role in molecule-surface interaction. Indeed, electronic states in the entire d-band of the metal are crucial for controlling the reactivity of the surface.

Thus, it is important to consider all the fundamental attributes of the d-band, such as its average energy, filling and width. [21] Mn with five d-electrons is the only transition metal that

have a ferromagnetic coupling. However, the study of magnetic properties is out of scope to present study.

Scanning tunneling spectroscopy (STS) is a key tool for accessing properties of organometallic molecules adsorbed on surfaces. It usually probes the electronic states of a surface, which are located within a few eV on either side of the Fermi level. [22] However, the rich variety of signatures complicates the identification of its origin, i.e. determining whether a feature is intrinsic to the molecule, relevant for a metal−ligand interaction or related to the interaction of the molecule with the substrate. [23]

When acquiring dI/dV curves (i.e., the energy resolved density of states at a particular sample spot), one of the fundamental problems is the electronic contribution of the tip. Tip characterization is essential to obtain trustworthy data and rule out the influence of the tip sharpness and possible attached impurities. For noble metals (Ag, Cu and Au) measuring the substrate's surface state is a standard way to check the tip quality. If the observed signal is practically flat except for a step function matching the position of the surface state band bottom, then the tip is considered proper for doing spectroscopy measurements. For Ag (111) the step is observed close to -65 meV and is identified as the surface state onset. This quality test of the tip is done on the substrate (away from the molecular islands) before and after each set of measurements, which we name hereafter as Ag spectroscopy. In appendix 4 different Ag spectroscopies are showed, clearly corresponding to different tip configurations.

To study the electronic configuration of the coordinated phase we perform point spectroscopy measurements on the three interesting locations identified in the topography: the Mn ions and the two-ligand types between the tetramers. The latter will be denominated as big and small lobe depending on their topographic intensity, as marked in Fig. 3.3.

The dI/dV spectra that were taken on top of the Mn ion show a prominent peak at 1.8V. This feature is common to the other spectra shown on Fig. 3.3, but exhibits the biggest intensity on the Mn ion. Thus, we attribute this peak to a delocalized orbital along the whole molecule. According to Ref. [24], this peak comes from a hybridization of 3d metal and organic states of the molecule. The HOMO orbital, related to the peaks near Fermi level (at -0.025 V), is formed mostly by Mn 3d states with a slight contribution from C 2p orbitals. [24]

In the molecular lobes that correspond with the DCDAE monomers in topography, apart from the 1.8 V peak, we observe an additional prominent peak around 0.8 V. Even when this peak is quite clear for the big lobe case, which in topography is observed as a single broadened blob, the peak at 1.8 V is still dominant. In the big lobe point spectroscopy, we can further observe a small peak at 0.2 V, which is missing in the small lobe dI/dV spectrum. For the small lobe, the peak close to 0.8 V is comparatively smaller that the extended orbital found at 1.8 V, although sharper than the big lobe case.

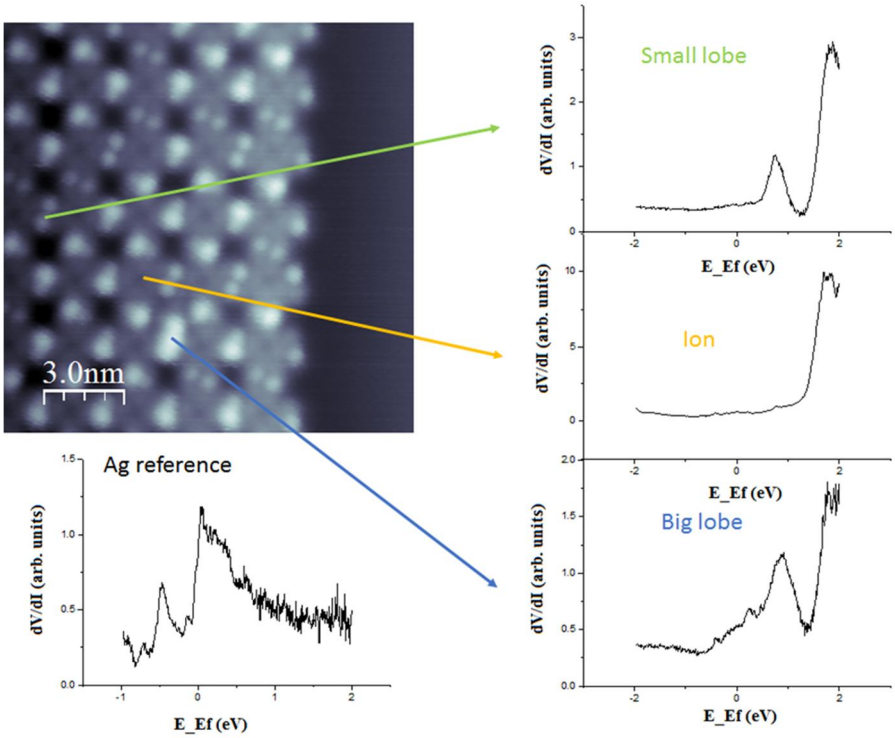

Fig 3.3. Point spectroscopies at relevant topographic positions marked by the origin of the arrows. The bottom axis shows the energy difference with respect to the Fermi level. The spectrum named as Small lobe (in green) corresponds to the signal between two small features. Ion spectroscopy (yellow) is acquired at the manganese ion. Big lobe (blue) shows the spectroscopy between the bigger and brighter features. The spectrum in the bottom-left shows a Ag reference spectroscopy, which is taken outside the square network and shows the expected step feature at -65 mV corresponding to the onset of the Ag(111) surface state. Note that there is no relevant features above the Fermi level, which excludes tip related artifacts in the spectroscopy of the molecular network for the unoccupied region (positive bias).

The bias-dependent STM images of single molecules suggest that, if the distribution of molecular orbitals can be detected simultaneously in the real and energy spaces, we will obtain comprehensive information about the electronic states of a single molecule. The STM dI/dV mapping technique just meets this requirement. It integrates energy-resolved tunneling spectroscopy, which was known as scanning tunneling spectroscopy (STS) previously, into a spatial-resolved imaging procedure by STM. Making use of this technique, one can further examine the molecular orbital itself and obtain information about the electronic states of a single molecule, achieving spatial and energy resolution simultaneously. [25]

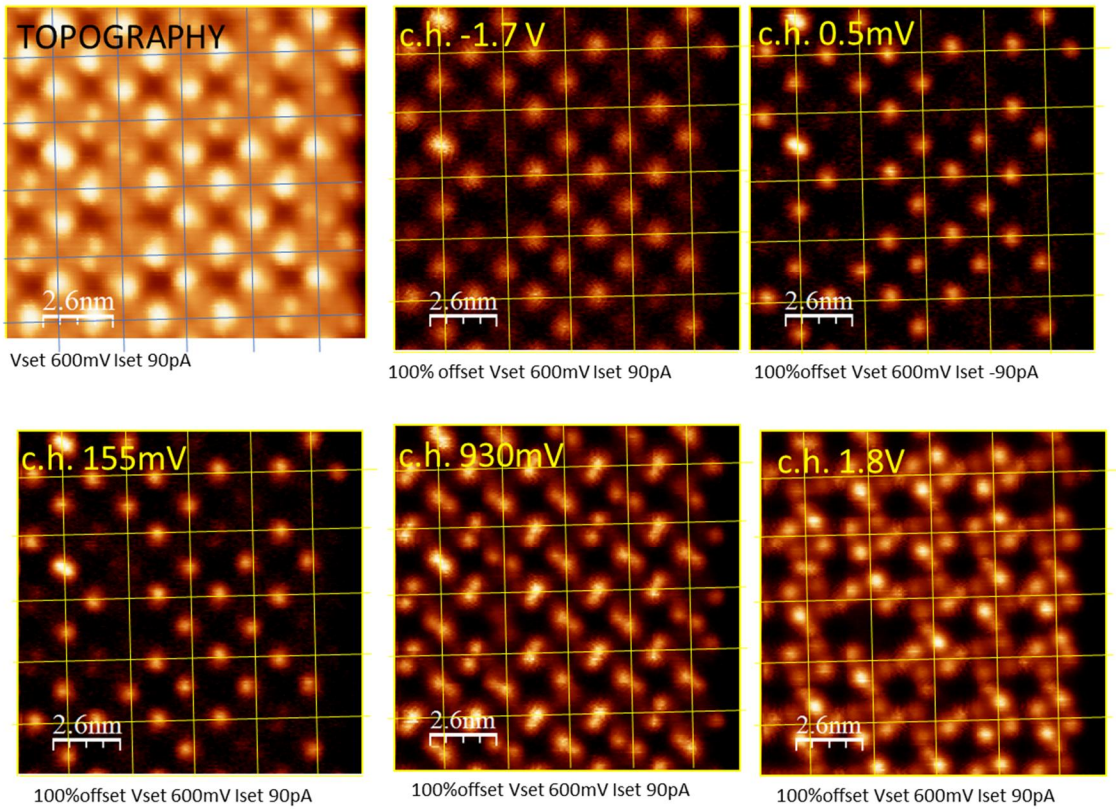

Fig 3.4 Topography and dV/dI maps at different voltages ranged from -1.7V to 1.8V. The corresponding values are indicated at the top of each image. A grid centered at the Mn atoms is added for easier visualization. Note that the grid position shifts slightly due to thermal drifts occurring during the data acquisition. Scanning details: setpoint before feedback opening at V=+600 mV and I=9 pA.

In order to get more information about the distribution of the local density of states (LDOS) of the coordinated network, spatial conductance maps at different energies was performed (Fig.

3.4). These dI/dV maps are measured at constant height of the tip (feedback open) at selected bias voltages determined by the spectroscopic features shown in Fig. 3.3 The *dI*/*dV* signal provides information about the surface and molecular LDOS and the spatial variation of electronic wave functions. [26]

The dV/dI maps in figure 3.4, correspond to selected bias voltages ranging from -1.7 to 1.8 V. In these we can observe three dominant structures: The first one, observed at voltages of -1.7V, 0.5mV and 0.155V, correspond to circular features located at the frontier between two DCDAE coordinating to different Mn ions. This signal corresponds to an HOMO state that is broadly spread over a huge energy range that crosses the Fermi level. This is a consequence of the hybridization of the state with the surface electrons, which dominates the topography for biases lower than 0.2V (not shown).

The second dominant structure is associated to the peak close to 0.8V, which corresponds to the LUMO of our molecular network. Its localization can be observed in the map at 0.93V. As expected, it falls into the lobes position. The onset of this orbital is already visible around 0.1V judging from the dI/dV spectra of Fig 3.3. The topography acquired at 0.6 V in Fig. 3.4 displays a mixture of the HOMO and the LUMO.

The third structure, can only be observed in the 1.8V map in Fig. 3.4, but it is shown in more detail in Figure 3.5. Intriguingly, at the DCDAE sites where the 0.93V maps have a minimum the state at 1.8V exhibits a maximum and viceversa. We believe that this reversal of the spectral weight between the orbitals at 0.93V and 1.8V corresponds to two isomer configurations, i.e., open or closed ring status of the diarylethene part of molecule (see Fig. 2.1), on the basis of the following reasoning:

1. A change in the position of the two hydrogens cannot justify such strong transfer of spectral weight between two orbitals. This transfer is better justified by a scenario containing two different molecules, i.e. the open and close isomers, within the network.
2. The molecular model consistent with the energy resolved maps we have found is sketched in Fig. 3.5. and Fig. 3.2. In this model, the bright state at 1.8V appears in the position of the ring containing the cyano groups. This orbital is compatible with the mirror axis of the planar closed ring DCDAE isomer. However, the bright state at 0.93V appears at one of the existing sulphur positions. This breaks the mirror symmetry of the molecule and fits to

an open ring isomer conformation, whose thiophene units are free to rotate around the bond marked by blue arrows in Fig. 2.1.

This possible scenario we have just described suggests that switching between the two isomers could be attempted by pumping energy into the molecules equal to the difference energy between the two orbitals. Importantly, our results imply that the optoelectronic functionality of the DCDAE is preserved upon adsorption on the surface and formation of the ordered squared coordination network.

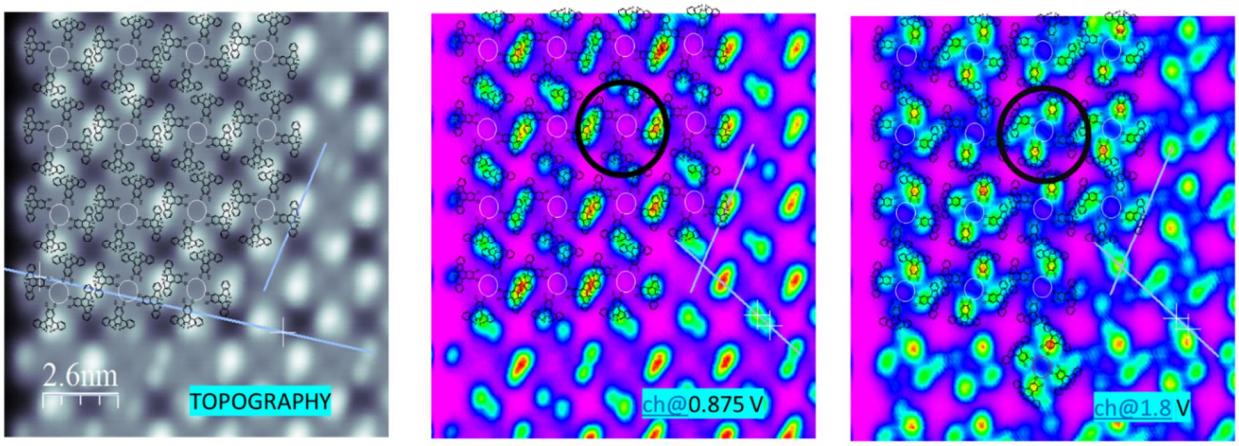

dFig 3.5. Topography and constant height dV/dI maps at 0.875V and 1.8V. In the image, the intensities for both bias voltages are visualized in a highly non-linear color scale and the tetramer model is overlaid. The observed maxima fall either at the ring containing the cyano groups (1.8 V) or at the sites containing the sulphur atoms (0.875V). Comparing both maps, the intensity maxima alternate their positions depending on the isomer configuration (open or closed rings). A good example of such behavior is highlighted by the black circle. Scanning details: setpoint before feedback opening at 60 pA and 0.6V.

3.1.3 Intermolecular interactions studied through tip manipulation.

The tip of the STM can be used not only as a scanning probe, but also as a tool to push or drag fundamental units. This is commonly known as atomic manipulation and we have employed it on our square coordinated network to study the dominant intermolecular interactions. Figure 3.6

shows the outcome of such tip manipulation, where we could separate a single tetramer from the rest of the coordinated network.

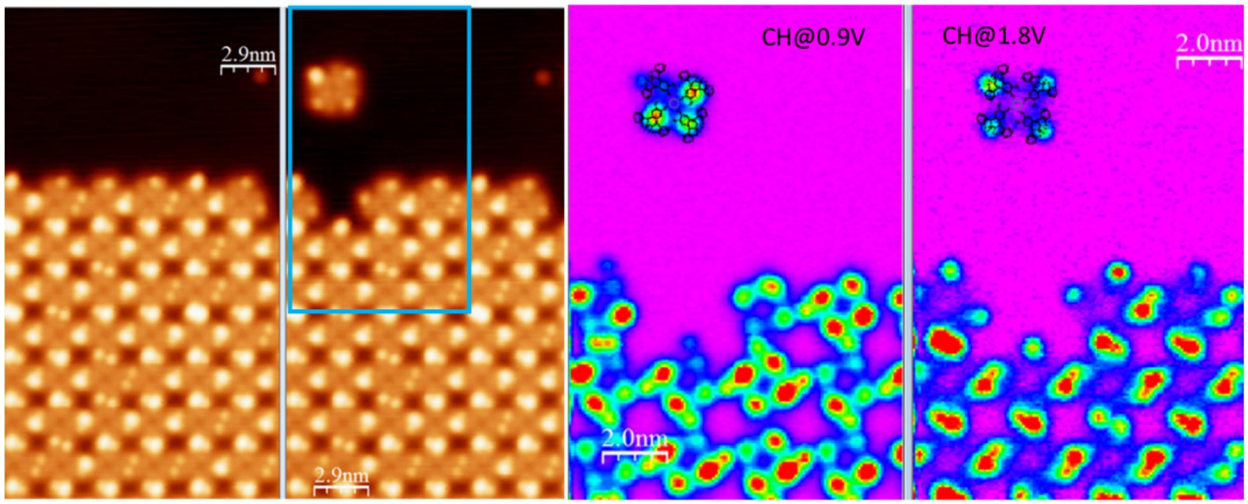

Fig 3.6. Molecular manipulation at the edge of the square network. A single tetramer was separated from the original network using STM manipulation methods. The STM tip is placed at a close vertical distance from the selected tetramer where chemical attractive forces are used to pull the object across the surface. As shown by the constant height maps at 1.8 V and 0.9 V, after the separation from the coordinated network, the tetramer maintains its original electronic structure (two types of molecules with either a bright lobe over the sulphur at 0.9V or over the cyano ring at 1.8V). STM regulation: V=600 mV, I=60 pA.

The manipulation was directed to the external molecule of the removed tetramer. This block movement allows us to conclude that these units are strongly bonded to each other through the Mn ion, but weakly to neighboring tetramers and to the surface. This supports the idea that metal-organic coordination is stronger than electrostatic inter-molecular interactions, such as H-bonding or van-der Waals forces. The bonding between two adjacent molecules is due to H---S bonds between the S atoms and the H in the external phenyl ring. The S lone-pair of electrons share charge with protons from H atoms providing a weak interaction between adjacent molecules that defines the square network structure as showed in figure 3.2 and 3.6. Importantly, we observe that tetramers maintain the original lobular structure, since we observe that there is the exact amount, and in the same order, of small and big lobes after separation from the coordinated network (note that the isolated tetramer is rotated clockwise 45º after manipulation). In particular, the constant height maps of Fig. 3.6 agree with the ones in the previous figure, in the fact that for

0.93V only the external part of the molecule stands out, whereas for 1.8 V the brightest features translate closer to the Mn ion. Note again the intensity reversal at these two energies.

3.2 Cyclotetramerization of precursors into MnDCDAE.

From the coordinated square phase, we try to generate other structures by means of on-surface reactions, as described in Section 1.2. For such process, the sample temperature was stepwise increased until a modification of the surface structures was observed. Particularly, when the temperature reached 360 ºC we obtained the sought cyclotetramerization of the coordinated phase, as conceptually shown in Fig. 3.7 for an isolated molecule.

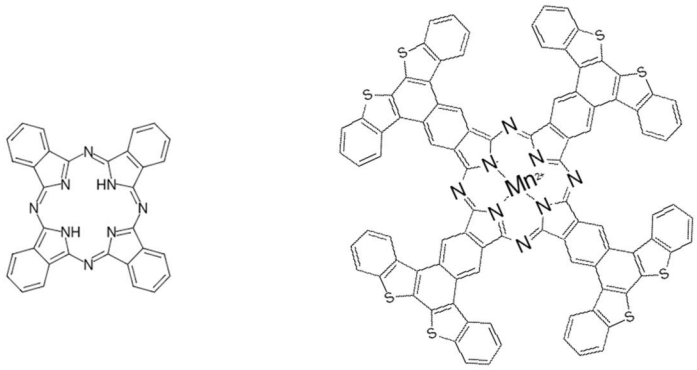

Figure 3.7. Comparison of a free-base (without metal center) phthalocyanine base (left) with a possible MnDCDAE product after on-surface synthesis (right).

The structure of the molecule is certainly bigger than the phthalocyanine base due to the presence of the diarylethene parts, as shown in figure 3.7. In this reaction, the cyano groups rearrange to generate the phthalocyanine core, resulting into a four-fold symmetric structure. Conceptually, all the functional groups from phthalocyanine and diarylethene molecules are expected maintain their original structures and therefore their original functionalities. In particular, the manganese ion should provide a magnetic signal that could affect to the molecule properties. However, as will be done in the following, such ideas must be experimentally demonstrated.

3.2.1 MnDCDAE zoology. Topographic observation of the existing ligands.

After the cyclotetramerization process, we observe that the square network is replaced by disarrayed molecular species that are randomly scattered over the surface (see Fig. 3.8). It is clear from the STM topography that not all molecular products are identical, but many molecular derivates coexist. This is clearly shown in Fig. 3.8, where the most characteristic species comprising different symmetries and ligand type were arranged close to each other by atomic manipulation. Note that not all precursors are observed to react, but this is a minor fraction in comparison with the amount of cross-like products found on the surface.

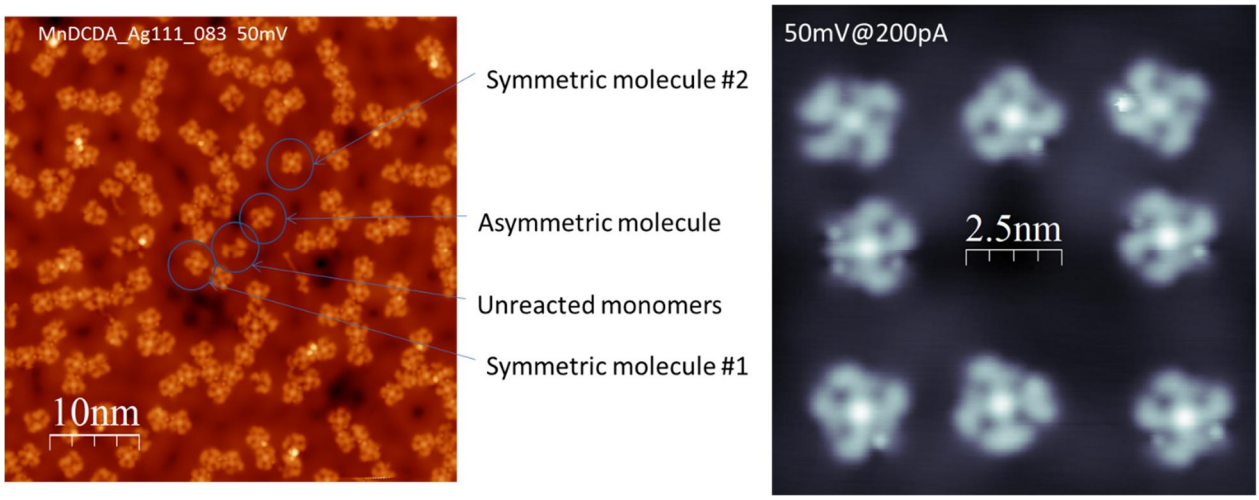

Fig 3.8 General view of the molecular products after the on-surface synthesis is shown on the left topographic image. The four circles identify different types of molecular species found on the sample: symmetric molecules #1 and #2, asymmetric ones and, unreacted monomers (without a manganese ion in the center). In the right image a set of different species are placed by atomic manipulation in proximity to one another. In both topographic images, we can observe a large number of molecule derivates, which is expected for products composed by four ligands each of which can take at least two different configurational states. STM regulation V= 50 mV, I= 200pA

By analogy to related systems, MnDCDAE molecules could be expected to adsorb in a flat geometry upon the metal surface in order to maximize the interaction with the substrate of the extended π-system and d orbitals of the transition metal at its center. [27] However, the presence of out-of-plane hydrogen in the DCDAE monomers provides the possibility to generate non-planar

geometries after the cyclotetramerization process. In such cases, the interaction with the substrate should be weaker, likewise affecting the STM measurements.

Focusing in the MnDCDAE zoology observed in Fig. 3.8, we observe more than two different ligand types at the external positions occupied by the diarylethene parts. Therefore, the big and small lobe description explained in section 3.1.1 for the coordinated phase simply falls short to account for these topographic images. In the molecular species found after cyclotetramerization, we should chemically expect the presence of open and closed ring isomers at the ethene and aryl groups (see scheme 3.7 right). This groups provide the photocromatic characteristic of this family of molecules.

Therefore, the number of molecular species found is very high. We can attribute this to the multiple combination of ligands with open and close ring on the four monomers that form a single molecule after cyclotetramerization. The two main classes of ligands are, seen at 50 mV, those with a bean shape and those featuring a sharp circular lobe. At each diarylethene position, the open isomer can take 3D shapes (pointing out from the surface or exhibiting different tilts) and also the out-of-plane H atoms (saturating the switching ring) can take two orientations in the form of small or big lobes. In consequence, the different options give rise to many combinations of lobes yielding the molecular product zoology exhibited in Fig. 3.8.

The complete geometry of the molecular species cannot be obtained simply from these topographic images. Even if STM can achieve atomic resolution, it is still limited to the external electronic cloud of the studied objects, which are generally extended when they are aromatic or feature hybridization processes (i.e., the molecular orbitals). Therefore, achieving full knowledge of the molecular structure is only possible using non-contact AFM and *ab initio* calculations of the molecular orbitals from these products.

3.2.2 Spectroscopy and dI/dV maps of selected cyclotetramerized species

The molecular structure at the central part of the molecule is always found to be symmetric. However, the status of the external ligands (open or close) and its spatial distribution on the substrate (influenced by the H out-of-plane orientation) must strongly affect not only the topology, but also the energy maps of each product. As explained previously, the molecular electronic structure will be significantly affected by hybridization between the d-orbitals of the central metal atom of the phthalocyanine and the neighboring nitrogen π-orbitals. In other words, the filling of

the d-shell of the central metal atom of the transition metal phthlocyanines influence the electronic structure of the macrocycle.

To obtain further insight into the local electronic structure of MnDCDAE species, we investigate by means of low-temperature high-resolution STS at different positions of selected molecules with different substrate orientations. Figure 3.9 and 3.10 shows a selected MnDCDAE molecule after cyclotetramerization and its corresponding point spectroscopies taken on the positions shown in the accompanying image.

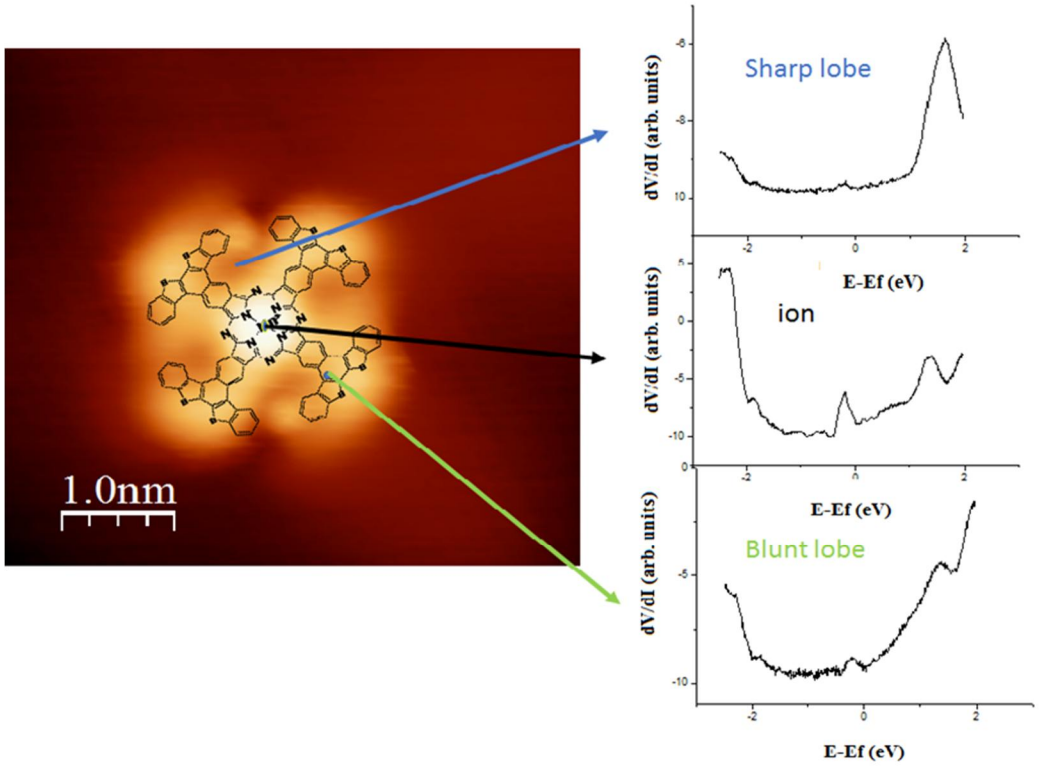

Fig 3.9 Point spectroscopies in relevant topographic positions of a MnDCDAE. Sharp lobe (in blue) correspond to the point where the peak at 1.5V is most prominent, which is between two adjacent monomers. Ion spectroscopy (black) correspond a molecule center just at the manganese ion, where we observe two peaks at -0.027V (HOMO orbital) and at 1.5V. Blunt lobe (in green) correspond to the middle of monomer and shows the same peaks that the ion spectroscopy but less defined. The molecule model overlaid in the topographic image is just a guide to the eye, since we cannot assign the ring status with the current dataset. STM image details: V= 50mV and I= 100pA.

The first important result is that the spectra are completely different to the square metal organic network (compare with Fig. 3.3), which exhibited peaks in the proximity of 0.8V and 1.8V. Now such peaks are missing and new clear features at sample bias of -0.027V, 1V and 1.55V show up. None of these are substrate related (cf. Fig. 3.3), so they can be safely attributed to the cyclotetramerized molecular product.

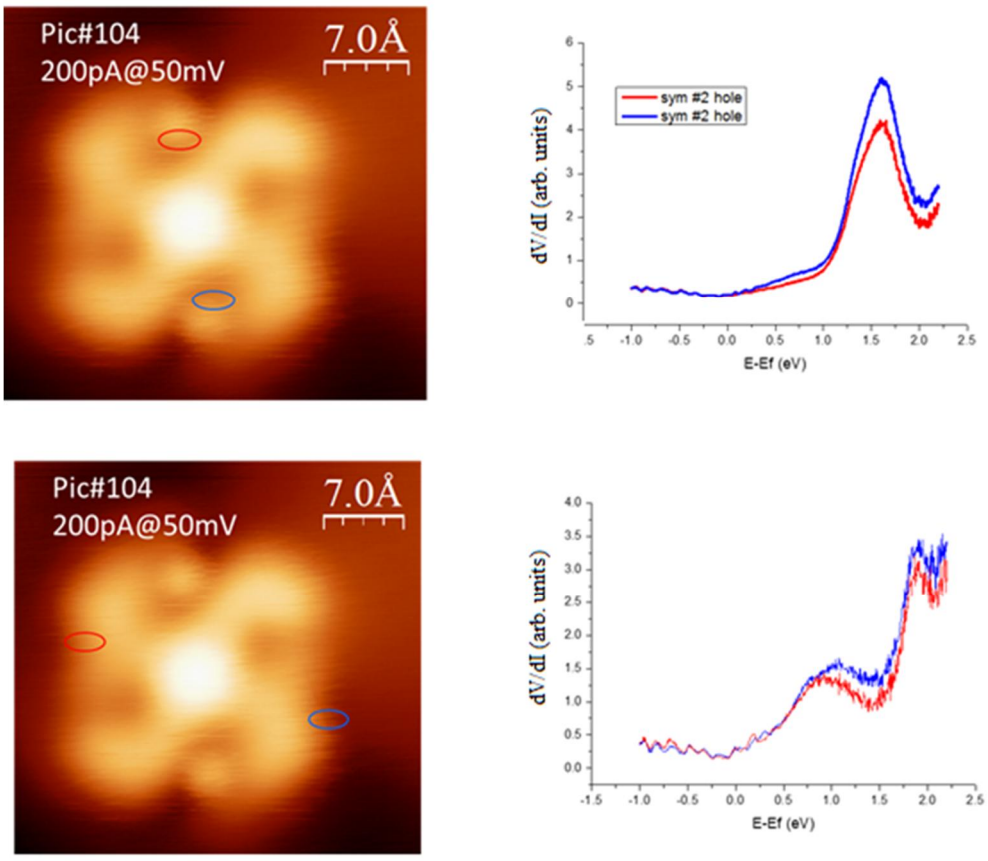

Fig 3.10. Average spectroscopies from the color coded areas taken from dV/dI grid maps. These correspond to complementary positions of the symmetric MnDCDAE molecule. The blue and red ellipses in the topographic images indicate the areas where the right spectroscopic curves are collected. Although there is a decrease in intensity, both curves of each graph are practically identical, as expected from the symmetry position they occupy with respect to the molecule center.

Both features at positive bias voltages, peaking at 1V and 1.55V correspond to the unoccupied states of the MnDCDAE molecules on the surface. They are found delocalized in several points of the molecule, and corresponds to extended orbitals in the covalently linked

structure we have created. For negative sample voltages the peak at -0.027V is mainly located around the Mn ion, and we attribute it to the highest occupied molecular orbital (HOMO). Aside from these peaks, in Fig. 3.10 we also find a strong feature at 2V, which is located at specific sites at the edge of the molecule, suggesting it is ascribed to a certain conformation of the isomer rings.

Based on the topography from the myriad of molecular species after cyclotetramerization (Fig. 3.8) we infer that there exist important variations of the density of states located at the edges of the molecule. While the LUMO at 1 V is distributed throughout the molecule periphery, and thereby should be affected by the open and close isomeric structures and relative distance to the substrate, we find that the HOMO is the same in all the different topographies and it is mainly located in the proximity of the Mn ion.

In order to understand the spatial distribution of dominant peaks for this particular molecule, we have acquired conductance maps at the relevant voltages. Fig. 3.11 shows that the best spatially defined peaks correspond to 1.5 V, which is located on the spherical-like lobes at the edge of the molecule. Similarly, the features at 1.0V and 1.9 V are located on the outer part of the molecule, but are complementary to the ones at 1.5V. This suggests, that the spherical lobes could be related to an open configuration, whereas the others belong to a closed situation. However, the presence of out-of-plane H atoms is prone to induce geometrical modifications that will locally show up on these maps.

In the unoccupied conductance maps of Fig. 3.11 the center of the molecule always shows a lack of intensity, even if peaks were observed in the spectra of Fig. 3.9. Such contradictory result can be easily explained as a relevant height difference between the outer parts of the molecules and its center, so that when the maps are acquired at constant current the tip is too far back from the molecule center to have the necessary sensibility to it. This is known as topography cross talk in density of states maps, which is avoided by working in constant height mode. Indeed, the Mn ion plays an important role on surface cyclotetramerization, as a significant charge donation from the underlying substrate to the central metal atom of the phthatlocyanine molecule leads to a redistribution of the 3d electrons including changes in the spectroscopy. [28] The HOMO peak at -0.027V is strongly localized at the Mn ion, which reflects its d-orbital character weakly hybridized with the conjugated orbitals of the organic parts. This orbital is dominant in topography at 50 mV

(Fig. 3.11 top panel). This is supported by the fact that for unreacted monomers or incomplete phthalocyanines, the HOMO relative to the Mn atom is absent on dI/dV spectra (see Appendix 5).

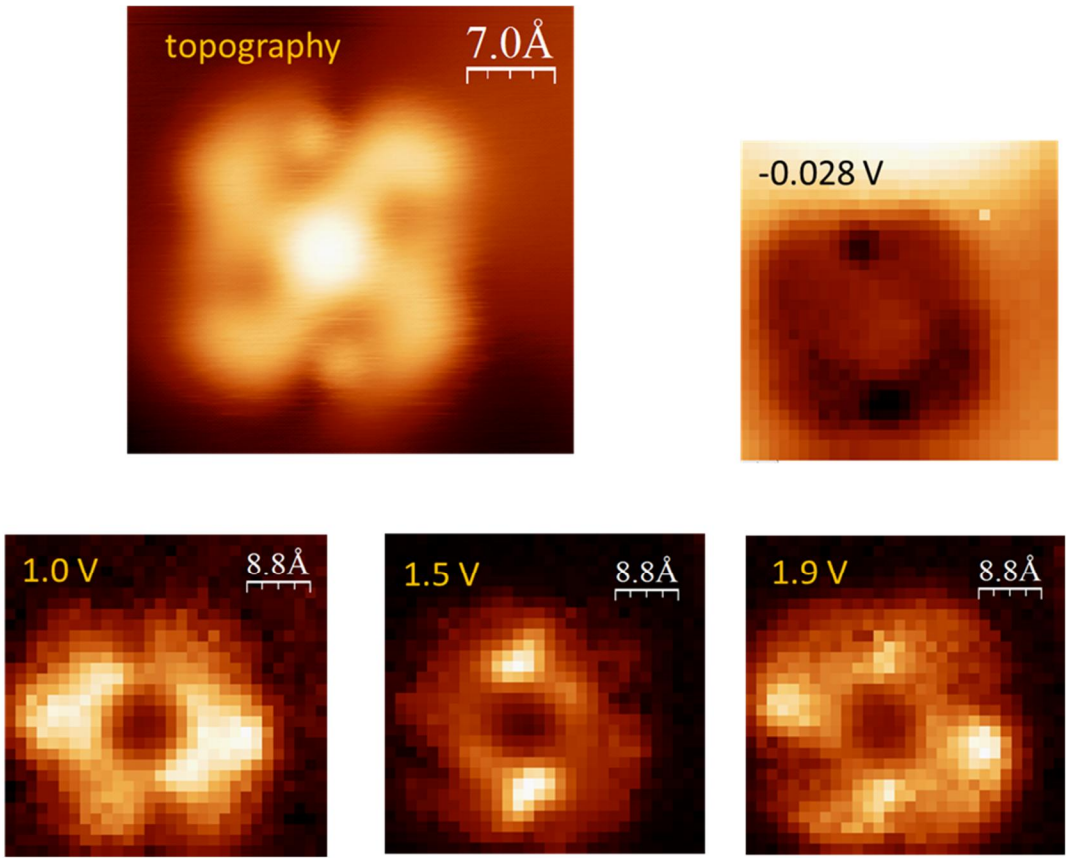

Figure 3.11. Constant current dV/dI maps at-0.028V, 1.0V, 1.5V and 1.9V for a single molecule. These maps were obtained from dense grid dV/dI curves recorded at each pixel of the single molecule image. For comparison, the molecule topography is showed in the image above. Scanning details: initial setpoint at 200pA and 750mV.

3.2.3 Switching of external ligands by tip pulsing.

After cyclotetramerization we have shown that different conformations of the diarylethene groups are possible on the obtained molecular species. Our next aim is to use the tip to manipulate and induce the switching of the external ligands. In this way, we use the STM tip as a tool to generate electric field induced switching by selective positioning it at a fixed height above a

molecule ligand with the feedback loop open and applying the desired pulse voltage, as showed by Wirth *et al*. [29] As a general rule, we find abrupt changes of the molecule conductance when the bias is ramped above 2V, that decrease in probability when the tip is gradually pulled away (i.e., the pulse must last longer to produce a conductance change as the tip-molecule distance increases).

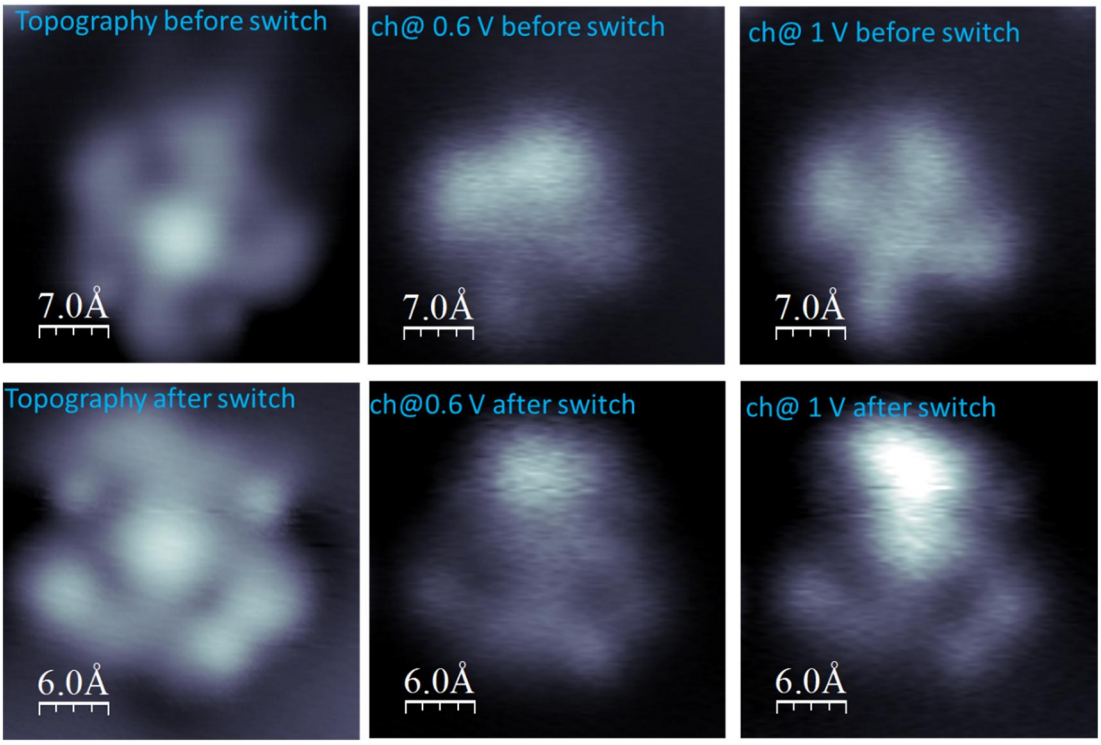

Fig 3.13 topography and constant height dI/dV maps at 0.6V and 1V before and after switching attempt to the top ligand. For switching, the bias was ramped from 0V to 2V with decreasing tip-sample distance until a jump in the current was observed. In the image after switching, a different topography from the original molecule can be appreciated that cannot be attributed to a straightforward bistable open or closed ring states. Instead, it resembles a broken bond between the central Mn ion and monomers as no union is appreciated in topography. The dV/dI maps do not show the four-fold continuous density of states in the vicinity of the Mn ion in sharp contrast to the original molecule (above).

Figure 3.13 shows such switching attempts on a selected molecule. The topographic images for a single molecule before and after the switch are showed in the left column of this figure and their corresponding constant height conductance maps at 0.6 V and 1V (probing the LUMO) are

shown at their right. The different electronic configuration in topography and in constant height images can be appreciated before and after the voltage pulse. In this case, the switching event of the ligand is not a smooth effect, but more like breaking up of the molecule. A possible explanation for such destructive mechanism is related to dissociative electron attachment, [30] where electrons with specific energies can be captured into the antibonding p* orbitals of the molecule, and then transferred into the s* orbital, causing bond breaking in the initial structure. Therefore, our switching attempt turns out to be unsuccessful as the structure of this molecule becomes quite different from the initial one.

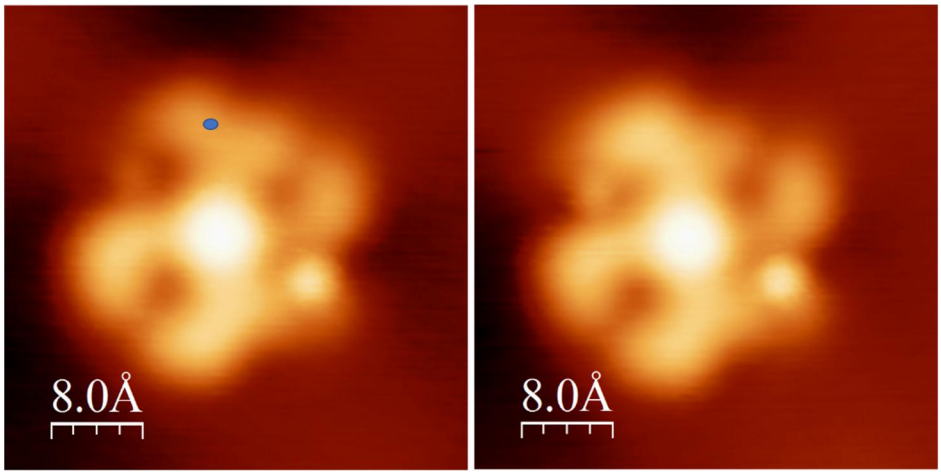

Fig 3.14 Successful switching following the recipe from Wirth et al. [29] The topographic images exhibit a contrast difference at the top ligands, which is attributed to the switching of the endgroups while conserving the original structure and the central ion bonds. A pulse of V=7V for 10s at z=5nm was applied over the blue dot showed in the left image.

Following the work by Wirth *et al*. [29] a different pulse methodology was used to trigger the ligand switching. Figure 3.14 shows the result of such new attempt consisting of applying a constant voltage of 7V for 10 seconds at a fixed tip-sample distance of 5nm. Note that the separation from the sample is so large that no tunneling current is expected. Interestingly, this new switching attempt turned out to be successful as the molecule kept its original structure while the ligand configuration does seem to change. However, after a successful switching event we were

unable to switching back the ligand to its original state, implying that the switch is irreversible for this ligand-surface combination.

Another interesting effect is that when we increase the pulsing strength (by ~2V pulse), irreversible changes occur not just in the molecular structure, but also on the substrate, as shown in Fig. 3.15. We observed modifications of the substrate LDOS induced by molecule dehydrogenation which results in a direct bonding of the molecule to the surface. The bonding of the C atoms whose hydrogens are removed, produce a LDOS uptake from the surface, as deduced from the dark regions around the modified molecules. After these changes, lateral manipulation of molecules is no longer possible as molecules are pinned to the surface. Such locking of the molecule-substrate proves that there is a bond formation between the C and the surface after hydrogen removal. Some examples of this phenomenon can be appreciated in figure 3.15. This experiment is relevant because it allows us to conclude that the out-of-plane hydrogens next to the sulphur atoms are still present even after the cyclotetramerization process occurs. Without these hydrogens, the only possible molecule configuration would be the closed bond with complete conjugated central ring, and so the ligand functionality would not be preserved in the new molecular species.

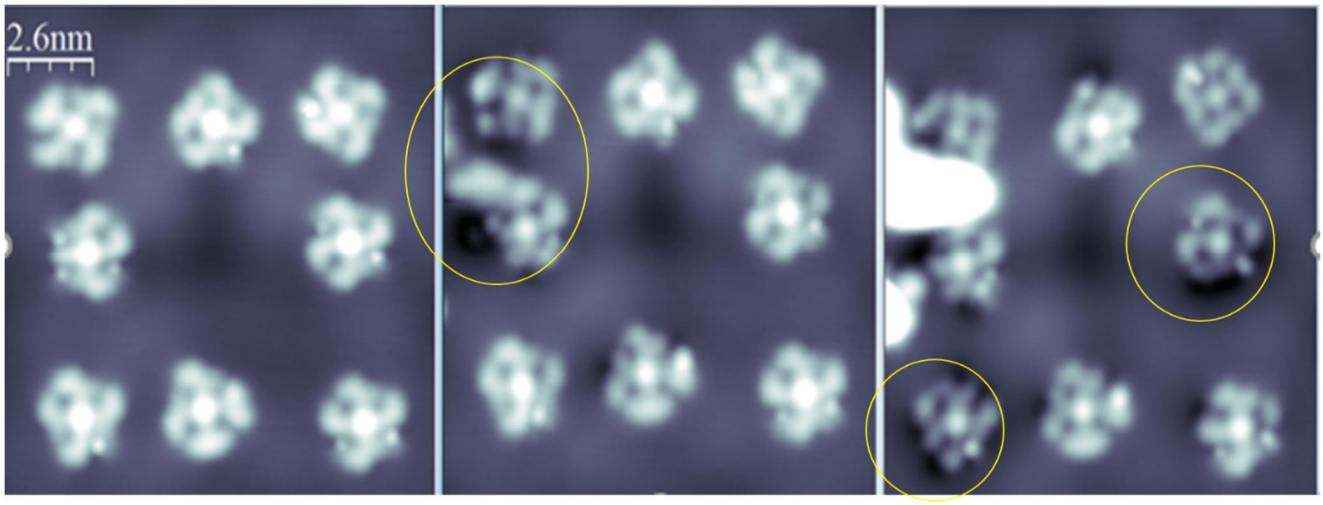

Fig 3.15. STM topographic images of the MnDCDAE zoology before (left) and after several consecutive switching attempts (center and right panels). The circles indicate where the switchings have been attempted. In the center and right image (yellow circles) we observe a depletion of the substrate LDOS (decreasing of the contrast) around the molecules, linked to the dehydrogenation process of the molecules, which is caused by C-substrate bond formation (in yellow).

4- OUTLOOK AND CONCLUSIONS

In this work, we study the morphology and the electronic structure of the resulting assemblies of DCDAE and Mn ions on a Ag(111) surface. The room temperature most stable structure is a metal coordinated square array that react into MnDCDAE Phthalocyanine products after an on-surface reaction. To carry out such studies we perform STM and STS experiments at low cryogenic temperatures.

The MnDCDAE close packed islands have been produced by simultaneous co-evaporation of the molecular precursos and Mn atoms on the Ag(111) surface. We obtained a coordinated network, where each single Mn ion is bonded to four cyano (CN) groups, each belonging to a different DCDAE molecule, that form tetramer structures.

The metal-coordinated phase is afterwards transformed by cyclotetramerization that converts the existing tetramers into individual Phthalocyannine molecules. This is achieved by annealing the substrate to 360ºC in UHV conditions. The products are stable molecules with interesting properties as they maintain the original features of DCDAE monomers and allows manipulation of the external ligands by electrical switching. This switching was performed by STM pulsing close to the molecular external ligands. However, these results are not ideal, since the switching process is found to lack reproducibility and is irreversible.

Although STM can achieve atomic scale resolution of the energy states of the molecules under study, to obtain full understanding and control of the atomic structure of the covalent species, non contact-AFM and theory studies are required.

As outlook we foresee several possibilities in order to develop new functionalities:

1. Modification of the molecular structure, in particular of the out of plane H for CH3 to avoid the dehydrogenation of molecules that occurs at high bias voltages (around ~2V).
2. Introduction of other metallic centers or ions to see how it affects the close packed structures and cyclotetramerization process, as well as the possible coupling of magnetism to the open or closed ring state.
3. Investigation of the magnetic signal of the molecules to improve the functionalities and explore new ways in the switching behavior.

4. Include a variety of external stimuli such as light, electric field, temperature, tunneling electrons and even chemical stimulus to activate molecular switching.
5. Synthesize the fully conjugated aryl group (i.e., without non-planar hydrogens and closed C-C bond) to answer to which state corresponds the wide lobe and the sharp circular lobe of the cyclotetramerized molecules.

In essence, we require further studies to create a molecular switch by on-surface synthesis of phthalocyanine-like devices.

REFERENCES:

[1] Kuhnle, A. Self-assembly of organic molecules at metal surfaces. Curr. Opin.Colloid Interface Sci. 14, 157–168 (2009).

[2] G. Franc, A. Gourdon, Covalent networks through on-surface chemistry in ultra-high vacuum: state-of-the-art and recent developments Phys. Chem. Chem. Phys. 13, 14283 – 14292 (2011).

[3] L. Bartels. Tailoring molecular layers at metal surfaces Nat. Chem. 2, 87 – 95 (2010).

[4] J. Sakamoto, J. van Heijst, O. Lukin, A. D. Schlìter, Angew. Novel Two-Dimensional Molecular Space Material with Regular Double Bonds Chem. Int. Ed. 48, 1030 – 1069 (2009); Angew. Chem. 121, 1048 – 1089 (2009).

[5] Robert Lindner and Angelika Kuhnle. On-surface reactions. ChemPhysChem, 16, 1582 – 1592 (2015).

[6] Javier Mendez, M. Francisca Lopez and Jose A. Martın-Gago. On-surface synthesis of cyclic organic molecules. Chem. Soc. Rev. 40, 4578-4590. (2011)

[7] CHRISTIAN G. CLAESSENS, UWE HAHN, TOMÁS TORRES. The Japan Chemical Journal Forum and Wiley Periodicals, Inc. Chem Rec 8: 75–97

[8] Victor N. Nemykina and Evgeny A. Lukyanets. Synthesis of substituted phthalocyanines. ARKIVOC (i) 136-208 (2010).

[9] Sun Y. S. Chow and Dennis K. P. Ng. Synthesis of an ABCD-Type Phthalocyanine by Intramolecular Cyclization Reaction. American Chemical Society.

[10] Stefano Tebi et ad. On-Surface Site-Selective Cyclization of Corrole Radicals. ACS Nano, 11, 3383−3391 (2017).

[11] Marten Piantek, David Serrate, Maria Moro-Lagares, Pedro Algarabel, Jose I. Pascual, and M. Ricardo Ibarra. Manganese Phthalocyanine Derivatives Synthesized by On-Surface Cyclotetramerization. *J. Phys. Chem. C*, *118* (31), pp 17895–17899 (2014).

[12] Galbiati, M. Molecular spintronics. 2016. Springer.com. Chap 2.

[13] http://www.chem.qmul.ac.uk

[14] http://www.topac.com/kcel.html

[15] http://angstromengineering.com/tech/electron-beam-evaporation

[16] Kenji Matsuda, Masahiro Irie. The use of Diarylethene Derivatives for Photo-switching. http://www.tcichemicals.com.

[17]. Harold J.W. Zandvliet and Arie van Houselt. Scanning Tunneling Spectroscopy. Annu. Rev. Anal. Chem. 2:37–55 (2009).

[18] Claudius MORCHUTT. On-Surface Assembly and Reactions of Organic Molecules in Ultra-High Vacuum. ÉCOLE POLYTECHNIQUE FÉDÉRALE DE LAUSANNE.

[19] C. Julian Chen Introduction to Scanning Tunneling Microscopy: Second Edition. 2007. Oxford Universtiy Press.

[20] E. T. Foley, N. L. Yoder, N. P. Guisinger, and M. C. Hersam. Cryogenic variable temperature ultrahigh vacuum scanning tunneling microscope for single molecule studies on silicon surfaces. © 2004 American Institute of Physics.

[21] Yutaka Wakayama. On-surface molecular nanoarchitectonics: From self-assembly to directed assembly. Japanese Journal of Applied Physics 55, 1102AA (2016)

[22] Dirk K Morr. Theory of scanning tunneling spectroscopy: from Kondo impurities to heavy fermion materials. Rep. Prog. Phys. 80, 014502 (18pp) (2017) .

[23] Lei Dong, Zi'Ang Gao, Nian Lin. Self-assembly of metal–organic coordination structures on surfaces. @ 2016 Elsevier Ltd. All rights reserved.

[24] I. Bidermane et ad. Atomic contributions to the valence band photoelectron spectra of metal-free, iron and manganese phthalocyanines. Journal of Electron Spectroscopy and Related Phenomena 205, 92–97 (2015).

[25] Randall Mfeenstra. Scanning tunneling spectroscopy. Surface Science.Volumes 299–300, 1 January, Pages 965-979 (1994).

[26] Shawulienu Kezilebieke, Anis Amokrane, Mathieu Abel, and Jean-Pierre Bucher. Hierarchy of Chemical Bonding in the Synthesis of Fe-Phthalocyanine on Metal Surfaces: A Local Spectroscopy Approach. J. Phys. Chem. Lett. 5, 3175−3182 (2014).

[27] Bin Li, Zhenyu Li, Jinlong Yang and J. G. Hou. STM studies of single molecules: molecular orbital aspects. Chem. Commun., , **47**, 2747–2762 (2011).

[28] Heiko Peisert Johannes Uihlein Fotini Petraki Thomas Chasse´. Charge transfer between transition metal phthalocyanines and metal substrates: The role of the transition metal. Journal of Electron Spectroscopy and Related Phenomena (2015).

[29] J. Wirth, N. Hatter, R. Drost, T. R. Umbach, S. Barja, M. Zastrow, K. Rück-Braun, J. I. Pascual, P. Saalfrank, and K. J. Franke, Diarylethene Molecules on a Ag(111) Surface: Stability and Electron-Induced Switching. *J. Phys. Chem. C, 119* (9), pp 4874–4883 (2015).

[30] Jia Lin Zhang,ab Jian Qiang Zhong,ab Jia Dan Lin,ab Wen Ping Hu,c Kai Wu,de Guo Qin Xu,adf Andrew T. S. Weeb and Wei Chen. Towards single molecule switches: Chem. Soc. Rev. 44, 2998 (2015).

APPENDIXES:

Appendix1. Quantum theory below STM.

From: Handbook of Measurement in Science and Engineering, First Edition. Edited by Myer Kutz. ©2016 John Wiley & Sons, Inc. Published 2016 by John Wiley & Sons, Inc. Cap 56 SCANNING TUNNELING MICROSCOPY. Autor. Kwok-Wai Ng

In quantum mechanics a particle is described by a wave function ψ(x) satisfying the time-independent Schrödinger equation:

$$-\frac{\hbar^2}{2m}\frac{d^2}{dx^2}\psi(x)+V(x)\psi(x)=E\psi(x)$$

where V(x) is the potential and E is the energy of the particle. The probability of finding the particle in the range [a, b] is given by:

$$P(a\le x\le b)=\int_a^b \psi^*\psi\, dx$$

where ψ* is the complex conjugate of ψ. This probability allows the particle to be found even in the classical forbidden region and leads to the tunneling phenomenon.

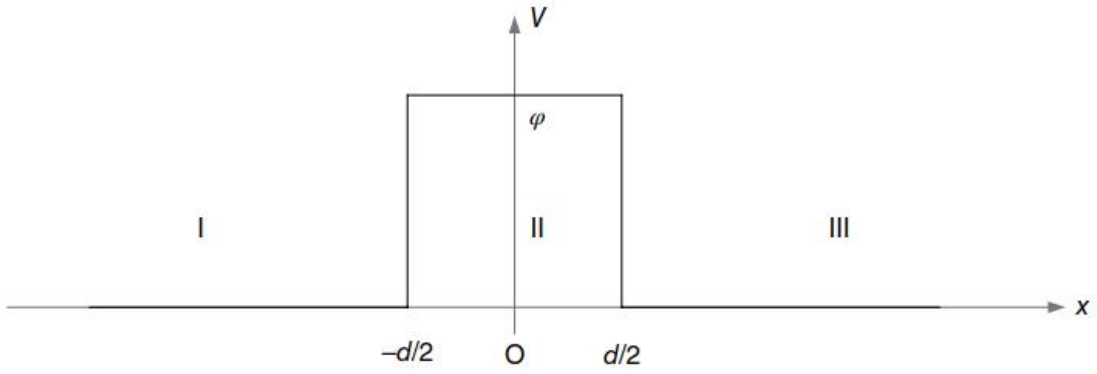

FIGURE 1 A square potential area of width d and height φ. In the discussion here the energy of the electron is less than φ, so the barrier is classically forbidden.

Consider a simple square potential as in the upper Figure: if a particle entering from the left with$E<V_0$, classically, it will be bounced back by the potential barrier. Quantum mechanically, solving Schrödinger equation for this potential will give the wave function of the particle as

$$\psi_{\mathrm{I}} = e^{ikx} + Re^{-ikx}$$
$$\psi_{\mathrm{II}} = Ae^{\kappa x} + Be^{-\kappa x}$$
$$\psi_{\mathrm{III}} = Te^{ikx}$$

$$\text{where } k = \frac{\sqrt{2mE}}{\hbar} \quad \text{and} \quad \kappa = \frac{\sqrt{2m(\phi - E)}}{\hbar}$$

The transmission coefficient is important here, and it can be derived from the boundary conditions in ψ and dψ/dx between the wave functions at x = −d/2 and x = d/2

$$|T|^2 = \frac{(2k\kappa)^2}{(k^2 - \kappa^2)^2 \sinh^2 \kappa d + (2k\kappa)^2 \cosh^2 \kappa d}$$

The fact that ψ III is not zero means there is a certain probability for the particle to tunnel through the barrier, giving rise to a probability current

$$j = \frac{i\hbar}{2m}\left(\psi \frac{\partial \psi^*}{\partial x} - \psi^* \frac{\partial \psi}{\partial x}\right) = \frac{\hbar k}{m}|T|^2$$

In low tunneling rate limit κd ≫ 1, sinh κd ~ cosh κd ~ e κd and T 2 ~ (2kk/(k2 +k2))2 e-2kd. While k and κ are mostly constant:

$$I \propto \exp(-2\kappa d)$$

the current is decaying exponentially with the barrier thickness d. A slight increase in d will produce a sharp drop in the current. For a reasonable tunneling rate, we require 2κd ~ 1. Roughly speaking, this means the barrier thickness d should be the order of the wavelength of the particle given by λ = 2π/k. The wavelength of a 1 eV electron is about 1.23 nm. If the barrier height ϕ is not a constant across the barrier, we can conveniently replace it with the average height because of the exponential dependence:

$$\kappa = \frac{\sqrt{2m\left(\bar{\phi} - E\right)}}{\hbar}$$

The preceding discussion can be applied to the real situation when two metals are separated by a vacuum gap (the barrier) of distance z. The barrier height will now become the average work potential of the metals at two sides. All conducting electrons of different energies at both sides will involve in the tunneling process. For simplicity we will ignore thermal excitation and assume the Fermi–Dirac distribution function is a step function (T=0 K). Only the electrons in the energy range $0 \le E \le |eV|$ at the left side in Figure 2 can tunnel because only they can find unoccupied states at the opposite side for tunneling to occur. If $\rho_L(E)$ and $\rho_R(E)$ are the electron density of states of the materials at the left- and right-hand sides in the figure, the tunnel current will be given as

$$I \sim \int_0^{eV} e\left(\frac{2k\kappa}{k^2+\kappa^2}\right)^2 e^{-2\kappa z} \cdot \rho_L(E)\rho_R(E)dE$$

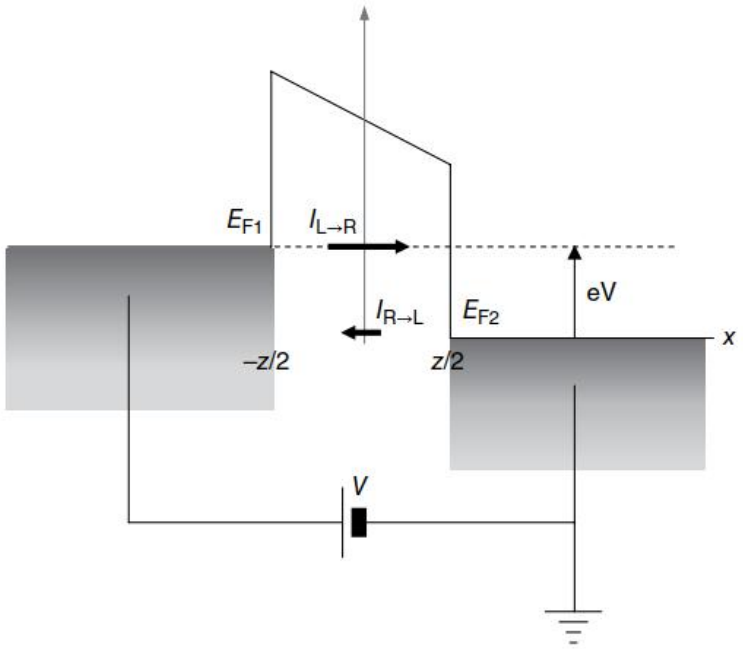

FIGURE 2 The Fermi level at one side of the barrier is raised by the applied potential *V*. This will tip the balance and create a net tunnel current through the barrier.

Note that the current is a convolution of the occupied and unoccupied density of states at both sides. Useful result can be derived if we assume the density of state of one material is more constant than the other, say, $\rho_L(\mathrm{E}) = \rho_L(0) =$ constant. The earlier equation can now be reduced to:

$$I \sim e\rho_{\mathrm{R}}(0)\int_0^{\mathrm{eV}}\left(\frac{2k\kappa}{k^2+\kappa^2}\right)^2 e^{-2\kappa z}\cdot\rho_{\mathrm{L}}(E)\,dE$$

Differentiating I with respect to d,

$$\frac{d}{dz}\ln I = \frac{1}{I}\frac{dI}{dz} = -2\kappa = -\frac{\sqrt{8m\left(\bar{\phi}-E\right)}}{\hbar}$$

From this equation, we can see how an STM can be used to determine the average work function of the two metals by a dI/dz measurement, where z is the sample–tip separation.

Besides the work function, STM can also be used to measure the density of state of a material. We should point out that the transmission coefficient is not as well understood and well predicted as described previously. This is especially true in the case of STM, when the wave

function is not really a plane wave and it is highly sensitive to the surface condition. For this reason, we will replace the transmission coefficient with an arbitrary function M (E, z), which plays the role of the tunneling probability matrix:

$$I \sim e\rho_{\mathrm{R}}(0)\int_{0}^{\mathrm{eV}}\left|M(E,z)\right|^{2}\cdot\rho_{\mathrm{L}}(E)\,dE$$

And

$$\frac{dI}{dV}\sim e^{2}\rho_{\mathrm{R}}(0)\left|M(\mathrm{eV},z)\right|^{2}\cdot\rho_{\mathrm{L}}(\mathrm{eV})$$

If the variation of M (E, z) is not as strong as ρ_L (E) and it can be approximated as constant in the energy range of measures, then the tunneling conductance dI/dV is proportional to the density of state ρ_L (eV). Tunneling spectroscopy is a powerful technique to measure the electron density of states in a conductor, and it is widely used to measure the energy gap and phonon spectrum in a superconductor. STM can also be used to measure the local density of state, and this type of measurement is known as scanning tunneling microscopy and spectroscopy (STMS). In the STM community, it is a common practice to rid the unknown proportional constant by dividing dI/dV with I/V and quote it as "normalized density of states," which actually equal to

$$\frac{1}{I/V}\frac{dI}{dV}=V\cdot\frac{e^{2}\rho_{\mathrm{R}}(0)\left|M(\mathrm{eV},z)\right|^{2}\cdot\rho_{\mathrm{L}}(\mathrm{eV})}{e\rho_{\mathrm{R}}(0)\int_{0}^{\mathrm{eV}}\left|M(E,z)\right|^{2}\cdot\rho_{\mathrm{L}}(E)\,dE}=\mathrm{eV}\cdot\frac{\rho_{\mathrm{L}}(\mathrm{eV})}{\int_{0}^{\mathrm{eV}}\rho_{\mathrm{L}}(E)\,dE}$$

The previous probabilistic current can be measured as an electrical current because electron carries charge. This tunnel current depends on the bias voltage and the sample–tip distance. For topographical imaging, the bias voltage should be set as high as possible to increase the tunnel current. However, this bias voltage should be less than the work functions of the sample and tip as field emission will replace quantum tunneling at higher voltages. The work function of most metals is in the order of a few electron volts. For this reason, the bias voltage used for most imaging work is between 0.1 and 1 V or slightly higher. With such a bias voltage, the tunnel current should be in

the range of nA (10−9 A) to pA (10−12 A). A greater current indicates direct touch between the tip and sample. Measuring a smaller current is pushing the limit of the electronics, and noise will eventually become intolerable. It is theoretically correct to use as small a tunnel current as possible. Since the tunnel current depends exponentially on the sample–tip distance, pulling back the tip by merely an angstrom will require a lot of reduction in tunnel current, so we should not compromise too much on the noise level in achieving a small tunnel current.

To measure such a small current, most STM put the first-stage amplifier as close to the junction as possible, in many cases just next to the tip or sample. This first stage amplifier is actually a current to voltage converter, converting the tunneling current to a few volts at the low-impedance output. This output can then be connected to the main electronics over long cables. Since the circuit is close to the junctions and very likely mounted on the STM body, it has to be simple with not too many components. Many STMs just use an operational amplifier to accomplish this, schematically shown in Figure.3.

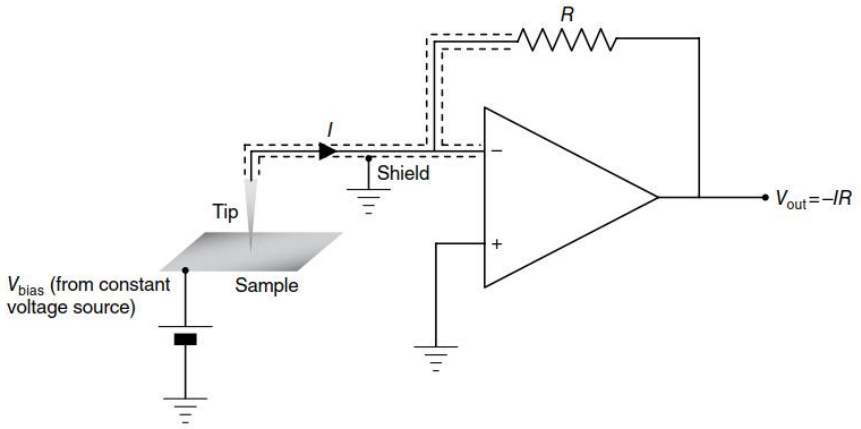

FIGURE .3 A current to voltage converter can be used to measure the tunnel current. The sensitivity is determined by the feedback resistance *R*. The operational amplifier has to be extremely low in input bias current.

Since the current is less than 1 nA with a bias voltage of 1 V, so the junction resistance is at least 1 GΩ. For this large load resistance, the bias voltage can be easily provided by a constant voltage source. In contrast, the junction resistance of a planar tunnel junction is often less than 10 Ω. Small-resistance junction should be current biased with a constant current source, so STM electronics is not very suitable for spectroscopic measurement of planar junctions. It is easier to

ground and guard the tip than the sample, so the tip in Figure 3 is virtually grounded, and the bias is applied directly to the sample. If the tunnel current is I, the output of this current to voltage converter will be −IR where R is the circuit feedback resistance of the circuit. In many cases, a logarithmic amplifier is used to remove the exponential dependence of the tunnel current. In constant height mode, this data will be recorded as the sample to tip distance, and its magnitude will be represented by a gray scale in the topographic image. In constant current mode, the output from the current to voltage converter will be compared to a preset value, and the difference or error will then be proportional, integration, and differentiation (PID) processed, magnified to high voltage and feedback negatively to the z-electrode of the scanner to maintain a constant tunnel current. The voltage to the z-electrode will be attenuated and recorded as the tip position that represents the topographic height.

In many experiments it is necessary to measure dI/dV for information in density of states. While one can do numerical differentiation on I/V data, it is preferable to measure dI/dV directly with a lock-in amplifier for a better signal-to-noise ratio. To do this a small sinusoidal modulation $\delta V \sin \omega t$ is added to the DC bias applied to the sample; the output of the converter will then equal to $(\delta I \sin \omega t)\, R$. Commercial STM electronics often provide external modulation input for this purpose. The modulation signal and the current to voltage converter output should be connected to the reference and voltage input of the lock-in amplifier, respectively. The output of the lock-in amplifier Vlock-in is DC and equals to the product of the amplitude of the sin ωt component in the input voltage and cosine of the phase difference between the input and reference voltage,

$$V_{\text{lock-in}} = -\delta I R \cos\phi = -\left(\frac{dI}{dV}\right)\delta V \cos\phi$$

so if δV is kept constant, Vlock-in is proportional to dI/dV. The phase of the lock-in amplifier can be adjusted for maximum signal when $\cos \phi = 1$. We now can measure I from the converter output and dI/dV from the lock-in amplifier output simultaneously. Note that for planar tunnel junction, when the junction resistance is small, current source has to be used, and δI will be the control variable, so only dV/dI can be measured in this case (fig 4).

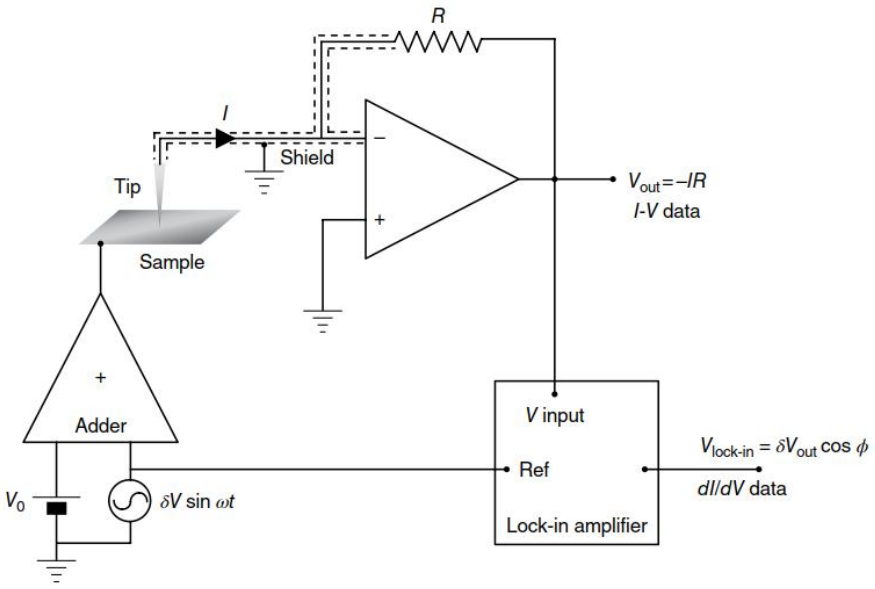

FIGURE 4 Lock-in amplifier can be used to measure *dI/dV*. A constant voltage modulation δV is added to the bias, and the lock-in amplifier is used to measure the resultant current modulation δI, which is proportional to *dI/dV*.

Appendix 2. Co-evaporation process.

(From Lei Dong, Zi'Ang Gao, Nian Lin. Self-assembly of metal–organic coordination structures on surfaces. @ 2016 Elsevier Ltd.)

Although the fundamental concepts of coordination chemistry are applicable in two dimensions, the coordination configurations in SMONs (Surface metal-organic networks) are markedly different from the conventional 3D ones. Firstly, the number of ligands attached to the metal ranges from 2 to 9 in 3D, depending on the size, charge and electronic structure of metal ions and ligands. However, for a metal atom adsorbed on a surface, the number of attached ligands is normally reduced as compared with the 3D systems because the space underneath the surface is inaccessible. Secondly, due to the 2D confinement, the most common tetrahedral or octahedral coordination in 3D is replaced by planar coordination in 2D such as twofold linear, threefold triangular or fourfold square coordination. Thirdly, in the solvent-free environment in UHV, the assembly preferentially proceeds via neutral species. Under this condition, the charge neutrality of the SMONs must take into account and their close contact with the conducting surfaces. Last but not least, the organic molecules and metal atoms interact intimately with the substrate, which often

are subjected to adsorbate–surface bonding comparable to the coordination interaction between the adsorbates. Therefore, it is the balance between metal–molecule, inter-molecule and adsorbate–surface interactions to determine the structure of the SMONs. For example, even on relatively inert noble-metal surfaces, van der Waals forces or partial charge transfer between molecules and substrates often leads to a flat-lying adsorption geometry of planar aromatic molecules. Such a conformation imposes steric constraints that decrease the conformational freedom. Besides constraining molecular conformation, adsorbate–surface interactions also reduce the degrees of freedom of the adsorbates, for example, preventing the adsorbed molecules from flipping over.

The surface–adsorbate interaction features in energetically favored adsorption sites and molecular orientations with respect to surface atomic lattices (e.g. hollow sites and the [11-2] direction of Ag (1 1 1) surface). Hence, to minimize the free energy, SMONs often deviate from the 'ideal' coordination structures drawn from the coordination configuration. In some cases, these interactions are so distinctive that a metal surface could serve as a template to direct the structure of the SMONs. The surface–adsorbate interaction also means that the molecules and atoms must overcome the energy barriers for translational and rotational motion. As a result, the mobility of the molecules and atoms can differ by several orders of magnitude, which significantly affects the kinetic pathways of the self-assembly. Another important effect is that adsorbed metal atoms may alloy with or diffuse into the substrate at elevated temperature. These effects regulate the concentration of the metal atoms, which must be taken into consideration when assembling the SMONs at high temperatures.

Experimental details from the evaporation process:

In the following, a data of the parameters used in the co-evaporation process are described as a reference. These data are relative to equipment and can´t not be considered as absolute values.

Reaching UHV conditions: In order to obtain UHV, a system needs to be "baked", i.e. heated to high temperatures .The reason is that rest gas (mostly water) is adsorbed to the chamber walls and the vapour pressure from the water is so high that the system does not go into the UHV range. This also means that the water slowly desorbs and is thus pumped away but this takes a extremely long time at room temperature.

Outgassing are processes controlling the ultimate pressure and gas composition in high- and ultra-high vacuum system

Outgas DCDAE molecules: We apply a P_{set} (mW) from 130 to 220 mW until get a suitable presure.

Ag (111) sputtering: V= 1KV, I=10 mA, P = 3.7 $e^{-7}mbar$, Time 5 minutes.

Ag (111) annealing: V= 850 V I = 4.4 mA, T= 450-480 ºC P= 3 $e^{-9}mbar$ Time 6 minutes

Co-evaporation Mn + DCDAE.: Time 10 minutes. Pev=3.4 $e^{-9}mbar$

DCDAE evaporator setup: $\Delta f = -16\ hz/min$, $P_{sat} = 215\ mW$

Mn evaporator setup : Flux = 1.5 nA, Emission: I = 6.8 mA, V= 651 V.

Appendix 3. Self-assembly of monomer without Mn ion.

In this appendix a topography image and dV/dI maps at different bias voltages are showed for a self-assembled phase of DCDAE monomer evaporated in UHV in a Ag (111) surface. A complete different assembly is observed with respect to the square coordinated phase.

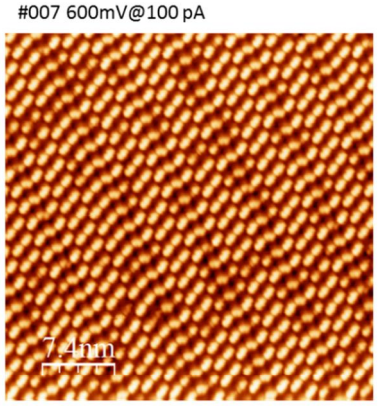

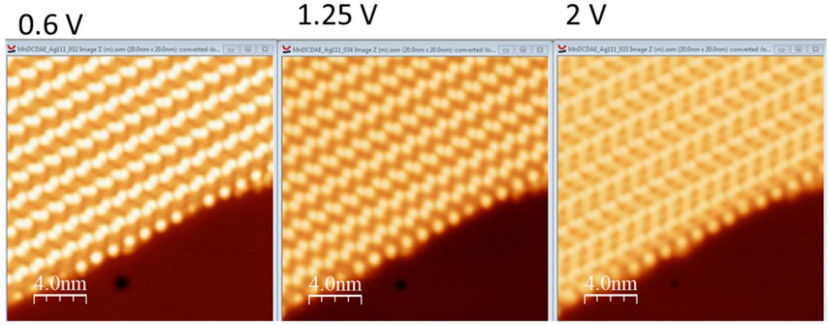

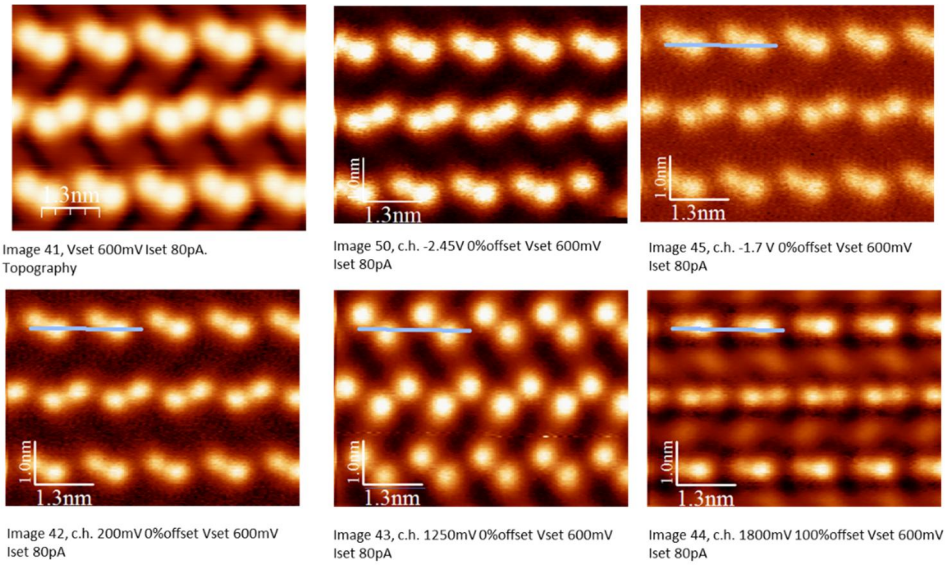

Image 41, Vset 600mV Iset 80pA. Topography

Image 50, c.h. -2.45V 0%offset Vset 600mV Iset 80pA

Image 45, c.h. -1.7 V 0%offset Vset 600mV Iset 80pA

Image 42, c.h. 200mV 0%offset Vset 600mV Iset 80pA

Image 43, c.h. 1250mV 0%offset Vset 600mV Iset 80pA

Image 44, c.h. 1800mV 100%offset Vset 600mV Iset 80pA

Appendix 4. Tip Ag spectroscopies.

Different spectroscopies taken outside the molecule shows the features related to STM tip and surface interactions, it depends mainly of the tip configuration that can change along the measurement process. The best practice is to measure the Ag surface reference spectra before and after a set of measurements in order to know if the tip changed during the acquisition process and to see how it affects the accuracy of the values obtained.

In the following we show some Ag reference spectroscopies measured in the course of these experiments that were used for calibrating our tip. We used exclusively those showing a clear step at the onset of the Ag(111) surface state:

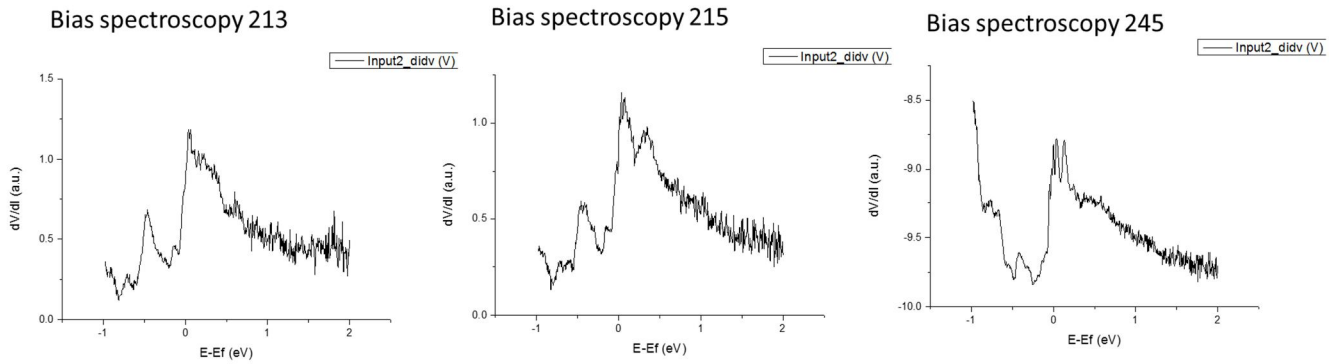

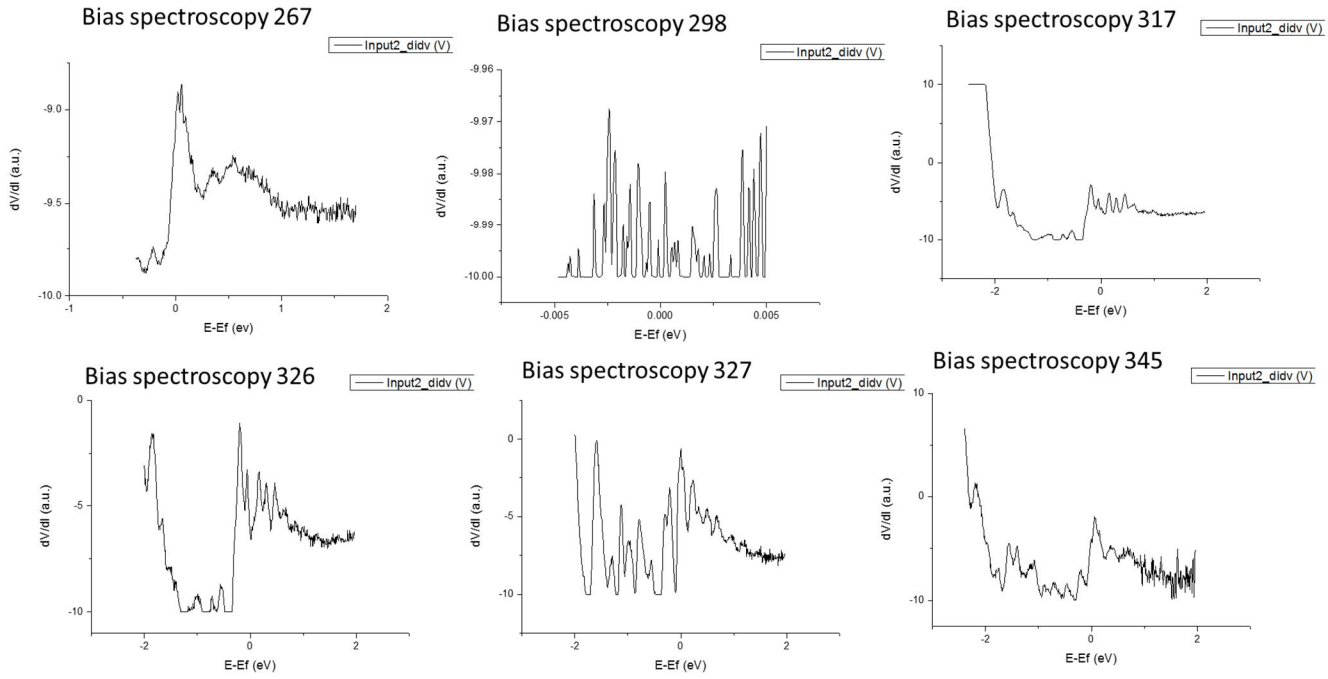

Appendix 5. Unreacted monomers.

The study of unreacted monomers found after cyclotetramerization can help shedding light on the Mn ion interaction with surface and with the side DCDAE monomers.

Unreacted molecules